

## Modeling insights into deuterium excess as an indicator of water vapor source conditions

Sophie C. Lewis,<sup>1,2</sup> Allegra N. LeGrande,<sup>3</sup> Maxwell Kelley,<sup>3</sup> and Gavin A. Schmidt<sup>3</sup>

Received 20 March 2012; revised 25 October 2012; accepted 26 October 2012; published 17 January 2013.

[1] Deuterium excess ( $d$ ) is interpreted in conventional paleoclimate reconstructions as a tracer of oceanic source region conditions, such as temperature, where precipitation originates. Previous studies have adopted coisotopic approaches (using both  $\delta^{18}\text{O}$  and  $d$ ) to estimate past changes in both site and oceanic source temperatures for ice core sites using empirical relationships derived from conceptual distillation models, particularly Mixed Cloud Isotopic Models (MCIMs). However, the relationship between  $d$  and oceanic surface conditions remains unclear in past contexts. We investigate this climate-isotope relationship for sites in Greenland and Antarctica using multiple simulations of the water isotope-enabled Goddard Institute for Space Studies ModelE-R general circulation model and apply a novel suite of model vapor source distribution (VSD) tracers to assess  $d$  as a proxy for source temperature variability under a range of climatic conditions. Simulated average source temperatures determined by the VSDs are compared to synthetic source temperature estimates calculated using MCIM equations linking  $d$  to source region conditions. We show that although deuterium excess is generally a faithful tracer of source temperatures as estimated by the MCIM approach, large discrepancies in the isotope-climate relationship occur around Greenland during the Last Glacial Maximum simulation, when precipitation seasonality and moisture source regions were notably different from the present. This identified sensitivity in  $d$  as a source temperature proxy suggests that quantitative climate reconstructions from deuterium excess should be treated with caution for some sites when boundary conditions are significantly different from the present day. Also, the exclusion of the influence of humidity and other evaporative source changes in MCIM regressions may be a limitation of quantifying source temperature fluctuations from deuterium excess in some instances.

**Citation:** Lewis, S. C., A. N. LeGrande, M. Kelley, and G. A. Schmidt (2013), Modeling insights into deuterium excess as an indicator of water vapor source conditions, *J. Geophys. Res. Atmos.*, 118, 243–262, doi:10.1029/2012JD017804.

### 1. Introduction

[2] The water cycle is a dynamic component of the global climate system and stable water isotopologs ( $\delta^{18}\text{O}$  and  $\delta\text{D}$ , expressed as a deviation from Vienna Standard Mean Ocean Water in permil, ‰, units) are valuable tracers of hydrological change. Isotopic variability in polar ice cores is commonly used to infer paleoclimatic information, such as past local temperature changes [e.g., *North Greenland Ice Core*

*Project members*, 2004; *EPICA Community Members*, 2006]. Deuterium excess ( $d$ ) is a second-order isotopic parameter linking  $\delta^{18}\text{O}$  and  $\delta\text{D}$  and has also been used to infer past changes in the atmospheric water cycle at Antarctic and Greenland sites [e.g., *Masson-Delmotte et al.*, 2004; *Jouzel et al.*, 2007; *Steffensen et al.*, 2008]. Deuterium excess indicates the deviation of a given data set from the Meteoric Water Line [*Dansgaard*, 1964], which represents the linear relationship between  $\delta^{18}\text{O}$  and  $\delta\text{D}$ , as shown in equation (1) [*Craig*, 1961]:

$$d = \delta\text{D} - 8 \times \delta^{18}\text{O}. \quad (1)$$

[3] During evaporation, kinetic nonequilibrium processes affect the relationship between oxygen and hydrogen isotopes and tag vapor with a  $d$  signature so that source conditions where vapor originates can be estimated [*Vimeux et al.*, 2002]. Proxy studies adopting coisotopic approaches ( $d$  together with  $\delta^{18}\text{O}$  variability) identify changes in both local temperature ( $T_{\text{site}}$ ) and in the oceanic source region temperature of precipitation ( $T_{\text{source}}$ ) [e.g., *Stenni et al.*, 2001; *Masson-Delmotte et al.*, 2005a, 2005b; *Stenni et al.*, 2010].

All supporting information may be found in the online version of this article.

<sup>1</sup>Research School of Earth Sciences, The Australian National University, Canberra, ACT, Australia.

<sup>2</sup>Now at School of Earth Sciences and ARC Centre of Excellence for Climate System Science, The University of Melbourne, Melbourne, Victoria 3010, Australia.

<sup>3</sup>NASA Goddard Institute for Space Studies and Center for Climate Systems Research, Columbia University, New York, New York, USA.

Corresponding author: S. C. Lewis, School of Earth Sciences, The University of Melbourne, Parkville, VIC, 3010, Australia. (sophie.lewis@unimelb.edu.au)

©2012. American Geophysical Union. All Rights Reserved.  
2169-897X/13/2012JD017804

[4] Proxy reconstructions that interpret  $d$  as an index of a single climatic variable (i.e., Tsource changes) adopt several fundamental assumptions that may not be valid under different boundary conditions, including that the seasonality of precipitation and relative humidity are largely invariant [Hoffmann et al., 2001; Vimeux et al., 2001]. Important complexities influence  $d$  and confound isotope-climate relationships, with field and experimental observations indicating that  $d$  values depend on parameters controlling the kinetics of phase changes during both evaporation and condensation, including source temperature, relative humidity, and wind speed [e.g., Merlivat and Jouzel, 1979; Jouzel and Merlivat, 1984; Cappa et al., 2003; Uemura et al., 2008; Luz et al., 2009]. Isotope-climate relationships depend on the stability of the moisture source to a site, the air-mass distillation history, and mixing, and hence these may vary on different timescales and under different boundary conditions [Masson-Delmotte et al., 2005b; Noone, 2008; Masson-Delmotte et al., 2011].

[5] Various types of isotope models have helped refine deuterium excess interpretations. In particular, the Mixed Cloud Isotopic Model (MCIM) is a distillation model used to constrain the relationship between  $d$  and temperature variability [Ciais and Jouzel, 1994] and to provide a quantitative assessment of the imprint of site and source conditions on isotopic variability (equations (2) and (3) after Stenni et al. [2001]; Masson-Delmotte et al. [2005a]). Combining MCIM results with back-trajectory analyses of air masses allows atmospheric circulation and moisture source changes to be inferred [Helsen et al., 2006; Schlosser et al., 2008]. Furthermore, the incorporation of water isotope tracers into dynamical complex general circulation models (GCMs) allows atmospheric vapor transport processes to be explicitly resolved and climatic influences on isotopic variability at Greenland and Antarctic proxy sites to be examined [Schmidt et al., 2007; Masson-Delmotte et al., 2008; Stenni et al., 2010].

[6] Isotope-enabled GCMs fitted with tagged water vapor tracers are useful for analyzing moisture histories under varying boundary conditions [e.g., Armengaud et al., 1998; Delaygue et al., 2000; Werner et al., 2001]. However, previous tagged water-type model studies show variable source region changes to high-latitude sites during simulated paleotime slices [Werner et al., 2001; Langen and Vinther, 2009] and Lagrangian source approaches [Sodemann et al., 2008;

Sodemann and Stohl, 2009) are limited in their ability to reveal evaporative source region variability in the past. Furthermore, previous GCM-based studies of the Last Glacial Maximum (LGM) water sources are largely based on proxy-derived sea-surface temperature (SST) estimates rather than simulated values [e.g., Delaygue et al., 2000; Werner et al., 2001]. As such, further research is necessary to understand past changes in high-latitude atmospheric circulation, moisture source region variability, and isotope-climate relationships.

[7] In this study, we examine the source of changes in deuterium excess over select ice cores sites in Greenland (GRIP and NGRIP cores) and Antarctica (EDC and EDML cores) over a broad range of simulated climate changes to improve our understanding of the relationship between deuterium excess and climate. We utilize a novel suite of generalized vapor source distribution (VSD) tracers as a complementary set of model diagnostic tools [Lewis et al., 2010] to examine this relationship. Region-specific numerical regressions (equations (2) and (3)) combined with VSD-enabled GCM simulations provide the opportunity to evaluate the robustness of deuterium excess as a proxy for source region temperature changes under different climatic conditions. We compare modeled  $d$  and Tsource values for ice core sites to synthetic  $d$  and Tsource estimates, applying the same numerical relationships [Stenni et al., 2001; Masson-Delmotte et al., 2005a] that link deuterium excess to surface conditions and have been used to interpret ice core records. We simulate mean climate conditions during preindustrial, mid-Holocene (6 kyr), LGM, and “water-hosing” time slices, together with changes occurring during simplified average El Niño- and La Niña-like conditions, as a broad representation of a variety of climatic changes. Using both simulated water isotope and VSD fields, we assess the skill of  $d$  as a proxy for temperature changes in the moisture source under various boundary conditions and examine the implications of seasonality for  $d$  interpretations.

## 2. Scope of Study

### 2.1. Site Descriptions

[8] Deuterium excess is investigated at a limited number of ice cores sites in Greenland (GRIP and NGRIP cores) and Antarctica (EDC and EDML cores) (Figure 1), which were selected based on the availability of MCIM-based quantitative climatic interpretations for comparison with

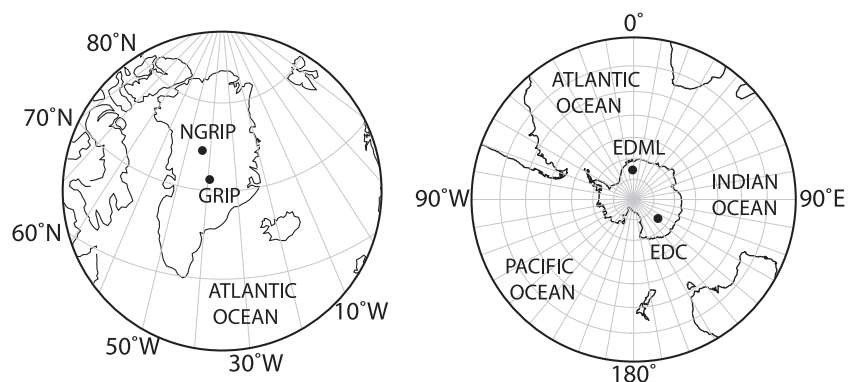


**Figure 1.** Map indicating location of selected Greenland (left, GRIP and NGRIP) and Antarctic (right, EDC and EDML) ice core sites.

VSD tracer results. The Greenland sites are located ~320 km apart and differ in elevation (2917 m at NGRIP and 3200 m at GRIP), accumulation rate (19 cm of water equivalent per year at NGRIP and 23 at GRIP), and deuterium excess (~10.5‰ at NGRIP and ~9.5‰ at GRIP) [Masson-Delmotte *et al.*, 2005b]. NGRIP (75°06'N, 42°19'W) is located downstream of GRIP (72°21'N, 38°18'W) on a common air-mass distillation trajectory [Masson-Delmotte *et al.*, 2005b]. GRIP and NGRIP provide an interesting basis for comparison, as dissimilarity between their isotopic ratios is attributed to a different mix of moisture sources to each site and hence regional-scale variations in advection toward Greenland [Masson-Delmotte *et al.*, 2005b]. In Antarctica, the EPICA Dome C (EDC; 75°06'S, 123°23'E) and Dronning Maud Land (EDML; 75°00'S, 0°04'E) sites also have different elevations (3233 m at EDC and 2780 m at EDML), accumulation rates (2.5 cm water equivalent per year at EDC and 6.4 at EDML; EPICA Community Members [2006]), and present-day (1960–1990 average) values of deuterium excess in snow (~9.3‰ at EDC and ~4.7‰ at EDML) [Stenni *et al.*, 2010]. The air-mass trajectories to these two sites are influenced by different oceanic basins (EDC faces the Indian Ocean and EDML the Atlantic Ocean; Stenni *et al.* [2010]), and hence separate climatic signatures in their respective  $d$  records may be deconvolved.

## 2.2. MCIM

[9] In studies utilizing the MCIM [Ciais and Jouzel, 1994], the model is tuned to simulate the deuterium-to-temperature slope along a pathway constrained by back-trajectory analysis and then run with varying site and source climatic conditions, including surface ocean  $\delta^{18}\text{O}$  ( $\delta^{18}\text{O}_{\text{sw}}$ ), relative humidity, wind speed and site temperature, and air pressure [Masson-Delmotte *et al.*, 2004]. Multiple linear regressions are then performed for site and source temperatures and isotopic variability over a specified region [e.g., Stenni *et al.*, 2001; Masson-Delmotte *et al.*, 2004, 2005a; Stenni *et al.*, 2010]. The inversion of simple isotopic models can then be used to infer site and source temperature fluctuations.

[10] Masson-Delmotte *et al.* [2005a] estimate the relative imprint of site and source conditions on isotopic variability over Summit, Greenland, as shown in equations (2-1) and (2-2):

$$\Delta d = -0.16\Delta T_{\text{site}} + 0.74\Delta T_{\text{source}} - 1.9\Delta\delta^{18}\text{O}_{\text{sw}}, \quad (2-1)$$

$$\Delta\delta^{18}\text{O} = 0.88\Delta T_{\text{site}} - 0.58\Delta T_{\text{source}} + 0.9\Delta\delta^{18}\text{O}_{\text{sw}}, \quad (2-2)$$

where  $\Delta$  indicates the deviation from modern (core top) conditions. The equivalent regressions for temperature and isotopic variability for EDC are adapted from Stenni *et al.* [2001] as shown in equations (3-1) and (3-2):

$$\Delta d = -0.50\Delta T_{\text{site}} + 1.30\Delta T_{\text{source}} - 2.60\Delta\delta^{18}\text{O}_{\text{sw}} \quad (3-1)$$

$$\Delta\delta^{18}\text{O} = 1.0\Delta T_{\text{site}} - 0.61\Delta T_{\text{source}} + 0.95\Delta\delta^{18}\text{O}_{\text{sw}}. \quad (3-2)$$

[11] These regressions are extended to EDML, where coefficients of regression are reported as similar [Stenni *et al.*, 2010], although it is noted that this may introduce minor errors into source and site estimates for this location. The last term ( $\delta^{18}\text{O}_{\text{sw}}$ ) is the ocean isotopic composition.

[12] It is not possible to calculate the full range of unknown source variables (temperature, relative humidity, and wind speed) using  $\delta^{18}\text{O}$  and  $d$ , so previous studies have applied varying coefficients describing the sensitivity of  $d$  to  $\Delta T_{\text{site}}$  to account for uncertainties [Uemura *et al.*, 2012]. As uncertainties cannot be calculated for all parameters, error ranges are not presented for regression coefficients, although these are detailed in some studies using simulations under different site and source temperatures [Stenni *et al.*, 2010], and the order of magnitude of coefficient uncertainties is typically 10–20% [Masson-Delmotte *et al.*, 2004]. Uncertainties in these coefficients include analytical uncertainty and uncertainties in the correction for  $\delta^{18}\text{O}_{\text{sw}}$ , tuning parameters and the restriction of evaporative conditions to  $\Delta T_{\text{source}}$  [Stenni *et al.*, 2010]. For the Antarctic equation set (3-1 and 3-1), the threshold for solid precipitation and the supersaturation function are tuned to correct the simulation of 1995–1996 average observed isotopic values [Stenni *et al.*, 2001]. Similarly, the Greenland relationships are tuned to fit GRIP mean modern isotopic values, with adjusted parameters controlling the supersaturation of vapor over ice and the proportion of condensate left in the cloud [Masson-Delmotte *et al.*, 2005a]. These relationships also assume that the  $d$  value of the sea-surface water is zero and that a constant relationship exists between condensation and surface temperature.

[13] Recent analysis demonstrates that different ranges of temperatures and selection of model isotopic output have substantial implications for the sensitivity of  $d$  to  $\Delta T_{\text{site}}$  [Uemura *et al.*, 2012]. Uncertainties in this sensitivity are attributed to changes in  $\Delta T_{\text{site}}$ ,  $\Delta T_{\text{source}}$ , and the gradient between these temperatures. Given the range of  $d$ - $\Delta T_{\text{site}}$  sensitivities that have been identified, the robustness of the isotope-temperature relationship derived from the MCIM is tested for a broad range of climatic changes using the isotope and VSD tracer modules of the GISS ModelE-R. Similarly, as the seasonality of high-latitude snowfall is an important control on isotopic variability in ice cores that cannot be assessed directly with ice core records [Masson-Delmotte *et al.*, 2005a, 2011], these relationships are also investigated in the winter and summer season to examine their robustness to seasonal variability.

## 3. GISS ModelE and Experiment Suite

### 3.1. Model Description

[14] Simulations were made using the coupled atmosphere-ocean GISS ModelE-R. The version used here is the same as submitted to the Coupled Model Intercomparison Project Phase 3, with the addition of water tracers. The horizontal resolution is 4° latitude by 5° longitude, with 20 vertical levels up to 0.1 hPa in the atmosphere [Schmidt *et al.*, 2006] and a 13-layer Russell ocean model of the same horizontal resolution [Hansen *et al.*, 2007]. Atmospheric advection uses a quadratic upstream scheme, with nine moments advected in addition to mean quantities. The ocean component is non-Boussinesq, mass conserving, and uses “natural” boundary conditions at the free surface.

[15] Water isotope tracers ( $^1\text{H}_2^{16}\text{O}$ , “normal” water;  $^2\text{H}^1\text{H}^{16}\text{O}$  or HDO, reported as  $\delta\text{D}$ ; and  $^1\text{H}_2^{18}\text{O}$ ,  $\delta^{18}\text{O}$ ) are incorporated into the atmosphere, land surface, sea ice, and ocean. Water isotopes are tracked through all stages of the

hydrologic cycle and are advected like water throughout the model, although at each phase change a fractionation is applied, explicitly determining equilibrium fractionation and with parameterizations accounting for kinetic fractionations [Schmidt *et al.*, 2005]. Schmidt *et al.* [2005] detail model isotopic fractionation processes, including the motivation for applying a parameterized supersaturation function ( $S = 1 - 0.004 \cdot T$ , where  $T$  is the temperature for the kinetic effect that occurs when condensing vapor to ice crystals in ice), to produce the correct relationship between  $\delta D$  and deuterium excess in Antarctic snow. Initial oceanic isotopic compositions are also prescribed ( $\delta D = \delta^{18}O = 0\%$ ).

### 3.2. Water VSD Tracers

[16] We apply a suite of water VSD tracers in the model, and atmospheric transport and condensation processes alter these analogously to a nonfractionating water isotope tracer [Kelley, 2003]. The VSD is the integrated mass of water vapor in each model cell and is expressed as an area integral of evaporative input unique to that cell. The VSD can be represented as a weighted sum of basis functions that are orthogonal to one another over the earth's surface. This study uses spherical harmonics as VSD basis functions, which are not anchored to any particular geographic boundary and require no prior definition of regions. The surface source of a given member of this new suite of tracers is equal to the evaporation field multiplied by its associated basis function. The sources of water vapor are traced back through any cloud processes to the site of surface evaporation. The precipitation source distribution is a subset of the VSD, defined where vapor condenses to liquid. We include 144 tracers that are resolved to wavenumber 11, providing an effective horizontal resolution of approximately  $8^\circ \times 10^\circ$ . It should be noted that factors such as land-sea contrasts cause real-world precipitation source distributions to vary unevenly, and hence the smooth spatial VSD patterns cannot be interpreted precisely on small spatial scales.

[17] In addition, we define 18 different geographic regions, and water evaporating from these regions is tagged

and followed throughout the simulations. These regional “painted water”-type tracers (hereafter regional tracers) are generalized from the VSDs and used primarily to investigate and quantify basin-scale vapor source changes between simulations. The reason that painted water tracers are not used globally at each gridbox is that this is computationally inefficient and 828 distinct tracers would be required to obtain  $8^\circ \times 10^\circ$  resolution.

### 3.3. Experimental Design

[18] Additional model tracers are computationally expensive and the VSD experiments take eight times longer to perform than comparable experiments with only water isotope tracers. Thus, experiments were conducted in two stages. First, coupled atmosphere-ocean simulations were conducted for a suite of experiment to provide a broad range of climatic changes with which to examine isotope-temperature relationships (Table 1). The first of these was performed and run to equilibrium (100s to 1000 years) for the preindustrial (0k), Holocene (6k), LGM (21k), and water-hosing (hereafter freshwater-forced) experiments. The simulated surface conditions from these experiments (SST and sea ice) as well as other changes (greenhouse gases, orbital parameters, and vegetation as necessary) were used as boundary conditions to drive the atmosphere-only version of the GCM with the VSD tracers incorporated in the second stage of the study.

[19] We also performed a series of simulations (El Niño-Southern Oscillation (ENSO+) and (ENSO-) where strong average idealized La Niña and El Niño surface temperature anomalies are imposed on the Pacific Ocean, using observational temperatures [Reynolds and Smith, 1994] and NINO3.4 indices over the period of 1981–2003 as surface boundary conditions. Monthly surface temperature anomalies associated with average La Niña (ENSO-) and El Niño (ENSO+) conditions were synthesized by correlating ENSO3.4 indices over this period with observed surface air temperatures (SATs) and were regressed to establish mean strong anomalies that are applied to SAT fields as surface boundary conditions for

**Table 1.** Summary of Model Boundary Conditions for Each Time Slice<sup>a</sup>

| Time (kyr BP)     | CO2<br>(fraction) | CH4<br>(fraction) | N2O<br>(fraction) | Perihelion | $\delta^{18}O_{sw}$<br>(‰) | Ice         | Other   | VSDs |
|-------------------|-------------------|-------------------|-------------------|------------|----------------------------|-------------|---|------|
| 0                 | 1                 | 1                 | 1                 | 2.85       |                            | No          |   | Yes  |
| 1                 | 0.98              | 0.87              | 0.94              | 349.6      |                            | No          |   | No   |
| 2                 | 0.98              | 0.81              | 1                 | 332.3      |                            | No          |   | No   |
| 3                 | 0.97              | 0.8               | 0.95              | 314.9      |                            | No          |   | No   |
| 4                 | 0.96              | 0.77              | 0.94              | 297.4      |                            | No          |   | No   |
| 5                 | 0.95              | 0.71              | 0.95              | 279.9      |                            | No          |   | No   |
| 6                 | 0.95              | 0.71              | 0.82              | 263.42     |                            | No          |   | Yes  |
| 9                 | 0.93              | 0.83              | 0.89              | 210.4      | 0.33                       | LIC         |   | No   |
|                   |                   |                   |                   |            |                            | ICE-5.2GLIC |   |      |
| 21 (LGM)          | 0.66              | 0.49              | 0.73              | 15.51      | 1                          | LIC         |   | Yes  |
| 21 (LGM ICE-5.2G) | 0.66              | 0.49              | 0.73              | 15.51      | 1                          | ICE-5.2G    |   | Yes  |
| Hosing            | 1                 | 1                 | 1                 | 2.85       |                            | No          | 1 Sv freshwater (T 0°C; S 0 psu; $\delta^{18}O$ -30‰)<br>x 100 model years over 50-70°N N. Atlantic | Yes  |
| ENSO+             | 1                 | 1                 | 1                 | 2.85       |                            | No          | El Niño-like average surface temperature anomalies  | Yes  |
| ENSO-             | 1                 | 1                 | 1                 | 2.85       |                            | No          | La Niña-like average surface temperature anomalies  | Yes  |

<sup>a</sup>Details are provided for 0, 1, 2, 3, 4, 5, 6, 9, 21, and 21k LGM-ICE-5.2G, freshwater-forced (hosing), ENSO+, and ENSO-, including greenhouse gases (Indermuhle *et al.*, 1999), perihelion in Julian days (Berger and Loutre, 1991), mean global  $\delta^{18}O_{sw}$ , and ice sheet boundary conditions.

the 0k simulations (Supplementary Figure 1). This method produces surface temperature conditions that are broadly representative of positive and negative phases of ENSO, although the regression was multiplied by a factor of 3 to ensure that the fingerprint of this type of climatic change is discernible throughout the high-latitude hydrological cycle (Supplementary Figure 2).

[20] The control simulation (0k) was run with all boundary conditions and atmospheric composition appropriate to the preindustrial period (ca. 1880). Experiments were also performed for mean climate conditions during the mid-Holocene (6 kyr BP, “6k”; *LeGrande and Schmidt* [2009]), the LGM (21 kyr BP, “21k”; A. LeGrande, personal communication), and a freshwater-forced event, as a highly idealized analog to a Heinrich event [*Stouffer et al.*, 2006; *Lewis et al.*, 2010]. In the 6k and 21k time slices, greenhouse gas concentrations were adjusted according to ice core reconstructions [*Indermuhle et al.*, 1999; *Brook et al.*, 2000; *Sowers et al.*, 2003] and seasonal insolation parameters [*Berger and Loutre*, 1991]. Surface ocean  $\delta^{18}\text{O}$  values are prescribed globally as 1‰ in the 21k simulation.

[21] The ice cap used for the 21k simulation is based on the ICE-5.2G reconstruction prescribed for PMIP2 simulations [*Peltier*, 2004], although we employ a modified Laurentide Ice Sheet model (ICE-5.2G-LIC; *Licciardi et al.* [1998]) that is considered most realistic for capturing LGM atmospheric circulation in the high northern latitudes (Supplementary Figure 1; D. Ullman, personal communication). A second 21k simulation was run with a standard ICE-5.2G [*Peltier*, 2004] boundary conditions as a comparison for the modified experiment. Hereafter, this experiment is referred to as LGM-ICE-5.2G so as to distinguish it from the primary simulation of the LGM.

[22] Water-hosing simulations are forced by a freshwater perturbation of 1 Sv (1 Sverdrup  $\equiv 10^6 \text{ m}^3/\text{s}$ ) added over 100 model years over 50°–70°N of the North Atlantic basin [*Lewis et al.*, 2010]. Each experiment was run for longer than 500 years in order to reach quasi-equilibrium, and mean climatologies over the last 100 years are present here. The LGM simulation was run for >800 years, although it did not fully reach equilibrium. Comparison of high-latitude surface conditions in this simulation with a complete LGM run confirmed the anomalies presented here are valid, although a secondary VSD-enabled run has not yet been conducted due to computational constraints. Results from the highly idealized freshwater-forced and ENSO-like simulations, and the LGM experiment, are not presented for climatic interpretations in their own right, but rather to assist in understanding  $d$ -climate relationships.

[23] For the second stage of these experiments, the atmosphere-only, VSD-enabled model was run for 6 years, with the final 5 years’ results reported here. A preindustrial coupled simulation with VSD tracers included was also conducted in order to test the validity of using results from atmosphere-only simulations, and this shows only small differences in precipitation source distributions. In addition to this suite of isotope- and VSD-enabled simulations, we consider an expanded series of Holocene time slice simulations made for 1, 2, 3, 4, 5, and 9 kyr BP [*LeGrande and Schmidt*, 2009], without corresponding VSD simulations. These experiments allow a comparison of simulated isotopic fields to be made with reconstructed proxy changes from ice core sites.

### 3.4. Definitions

[24] During each simulation,  $\Delta T_{\text{source}}$  values for each site for annual and seasonal (June–July–August (JJA) and December–January–February (DJF)) temporal averages were calculated as average surface temperatures within the simulated source region (including both land and ocean gridboxes, unless stated otherwise) using model VSD tracers, and modeled  $d$  values during these time averages are simply values occurring at gridboxes encompassing each ice core site. Corresponding “synthetic”  $\Delta T_{\text{source}}$  and  $\Delta d$  values were determined from equations (2) and (3) using modeled  $T_{\text{site}}$  and  $\delta^{18}\text{O}_{\text{sw}}$  fields, as a basis for comparison with modeled values. Climatological conditions within VSDs are calculated as averages weighted by the fractional amount of vapor contributed to the total precipitation.

[25] Climatic changes are reported as anomalies ( $\Delta$ ) relative to preindustrial (0k) simulation. Values presented for each ice core site (such as  $\Delta d$ ) are those occurring within single gridboxes, although are coherent with changes over a broader area unless otherwise stated. Climatological results from El Niño– and La Niña–like experiments are described as anomalies of ENSO+ phases relative to ENSO– ( $\Delta\text{ENSO}$ ). Southward and westward changes in mean moisture source locations to the sites are described by negative values, while northward and eastward shifts are described by positive values. All climatological anomalies reported are greater than 95% significant, given the control decadal variability about the 100-year mean.

[26] We define recycling as water with a continental, rather than an oceanic, evaporative source. The mean vapor transport distance (TD) is calculated as the distance (km) between the mean location of the precipitation source distribution and the ice core site. These values provide a minimum estimate of transport distances and do not consider the curved trajectories of air masses

### 4. Evaluation of Model Performance and Modeled Changes

[27] Extensive model evaluation of the GISS ModelE and its isotope module has been undertaken previously and showed that patterns of simulated preindustrial  $\delta^{18}\text{O}_p$  are highly correlated with observed fields [*Schmidt et al.*, 2005, 2006]. Large-scale simulated climate conditions and isotopic variability during the freshwater-forced [*Lewis et al.*, 2010] and mid-Holocene [*LeGrande and Schmidt*, 2009] experiments have also been assessed previously. Given prior model evaluation and the focus of this studying being the assessment of  $d$ -temperature relationships across a range of different climate states, we do not comprehensively compare simulated climatologies against observations for all experiments.

[28] The large-scale changes in simulated surface conditions across the suite of simulations are shown in Figure 2, and a summary of simulated site changes for the suite of experiments is provided in Table 2. Generally, discrepancies exist between simulated and observed climatological data in the high latitudes, with a warm bias occurring over Antarctica and a dry bias over Greenland resulting from deficiencies in the simulation of Northern Hemisphere (NH) storm tracks [*Schmidt et al.*, 2006]. Modeled precipitation patterns are generally closely related to observed

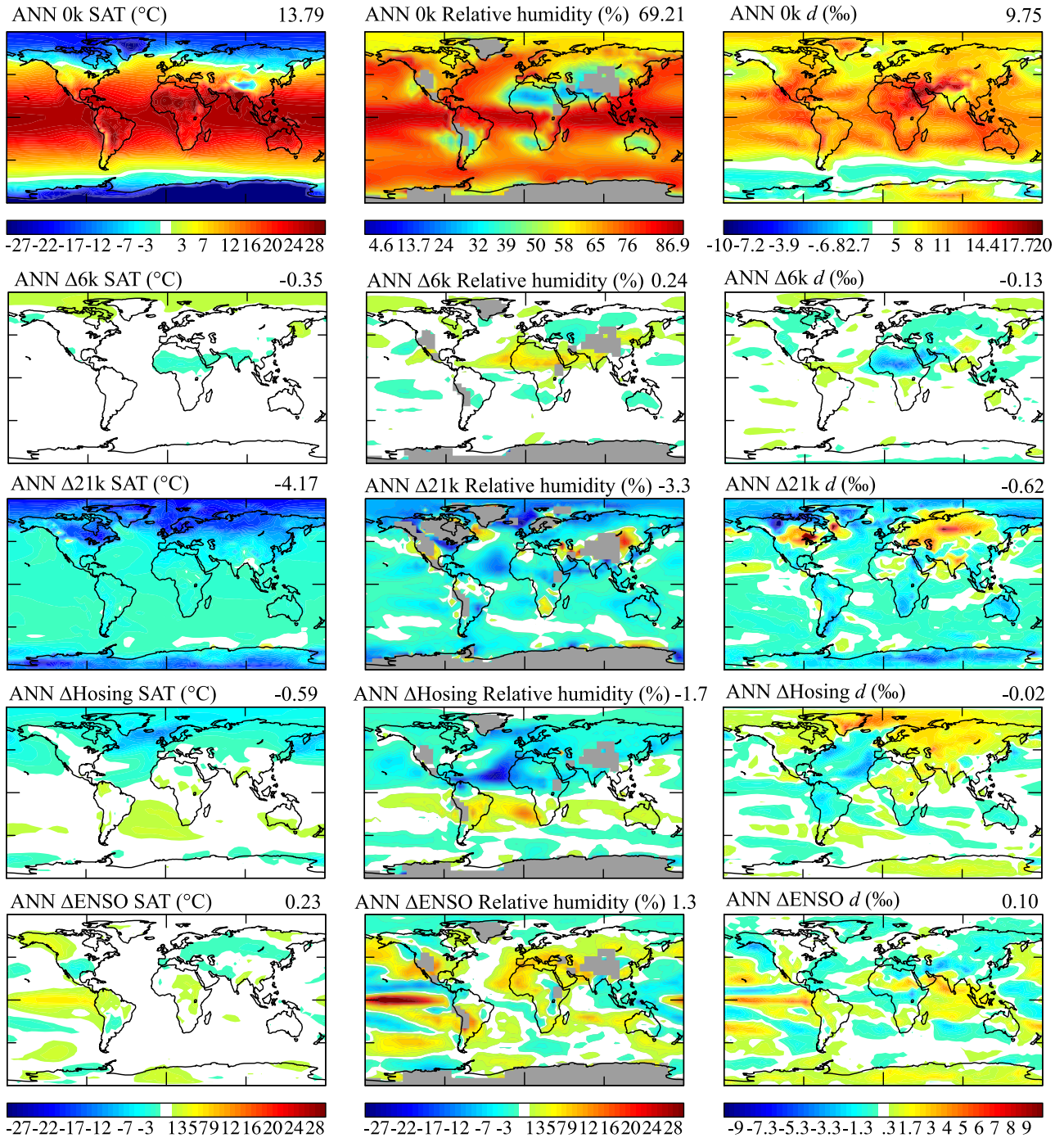


**Figure 2.** Annual average SAT (°C, left), relative humidity at 850 mb level (% , middle), and deuterium excess ( $d$ ) in precipitation (‰, right) for the control simulation (0k, upper) and anomalies relative to preindustrial for 6k, 21k, and freshwater-forced (hosing) experiments and ENSO+ minus ENSO- ( $\Delta$ ENSO) anomalies from the coupled simulations. Solid gray shading indicates areas of high model topography.

hydrological data, although simulated preindustrial snowfall is subdued relative to observations. These various climatic factors can also influence the relationship between temperature and isotopic compositions [Masson-Delmotte *et al.*, 2008, 2011]. However, the pattern of deuterium excess in precipitation is reasonably simulated, with the greatest discrepancies in hydrological fields occurring over the tropics, and isotopic values over Antarctica are generally enriched relative to observed [Schmidt *et al.*, 2007]. Overall,

we consider further analysis of simulated climates within the high-latitude regions to be valid, but focus on anomalies between experiments to account for these deficiencies.

#### 4.1. Comparison With Ice Core Sites

[29] A comparison of preindustrial simulated annual average surface characteristics ( $T_{site}$ ,  $d$ ,  $\delta^{18}O_p$ , accumulation, and precipitation) with observations at each of the four ice core sites is provided in Table 3. The simulated accumulation rate is

**Table 2.** Summary of Simulated Climatic Changes at Ice Core Sites GRIP, NGRIP, EDC, and EDML for 6k, LGM, Freshwater-Forced (Hosing), and ENSO-like Experiments<sup>a</sup>

|       |                  | 0k     |       |       | ANNUAL      |              |                 |               |
|-------|------------------|--------|-------|-------|-------------|--------------|-----------------|---------------|
|       |                  | ANNUAL | JJA   | DJF   | $\Delta 6k$ | $\Delta LGM$ | $\Delta Hosing$ | $\Delta ENSO$ |
| GRIP  | Tsite            | -29.9  | -16.5 | -39.8 | -0.1        | -12.2        | -6.2            | 0.3           |
|       | PR               | 0.1    | 0.2   | 0.1   | 0.0         | -0.1         | -0.1            | 0.0           |
|       | $d$              | 11.9   | 13.4  | 10.1  | 0.1         | -4.3         | 3.9             | -0.6          |
|       | $\delta^{18}O_p$ | -34.7  | -32.6 | -37.2 | 0.2         | -1.1         | -4.0            | 0.4           |
| NGRIP | Tsite            | -30.4  | -16.5 | -39.8 | 0.2         | -9.7         | -6.7            | 0.5           |
|       | PR               | 0.4    | 0.2   | 0.1   | 0.0         | -0.1         | -0.1            | 0.0           |
|       | $d$              | 12.8   | 13.4  | 10.1  | 0.2         | -4.9         | 3.5             | -0.2          |
|       | $\delta^{18}O_p$ | -34.9  | -32.6 | -37.2 | 0.1         | -0.9         | -3.7            | 0.4           |
| EDC   | Tsite            | -44.0  | -55.0 | -27.6 | -0.3        | -9.2         | -1.4            | 0.5           |
|       | PR               | 0.1    | 0.1   | 0.2   | 0.0         | -0.1         | 0.0             | 0.0           |
|       | $d$              | 6.7    | 7.8   | 6.0   | -0.3        | -5.3         | 0.6             | 0.4           |
|       | $\delta^{18}O_p$ | -38.2  | -40.1 | -37.1 | -0.1        | 1.1          | -1.5            | 0.0           |
| EDML  | Tsite            | -34.3  | -41.3 | -24.2 | -0.4        | -7.4         | 0.4             | 1.9           |
|       | PR               | 0.2    | 0.3   | 0.1   | 0.0         | -0.1         | 0.0             | 0.1           |
|       | $d$              | 9.5    | 9.5   | 8.3   | -0.6        | -3.5         | 0.8             | 1.9           |
|       | $\delta^{18}O_p$ | -39.3  | -40.5 | -36.2 | 0.3         | -0.1         | -0.3            | -0.7          |

<sup>a</sup>Details are provided for SAT of site (Tsite, °C), precipitation amount (PR, mm/day), deuterium excess in precipitation ( $d$ , ‰), and  $\delta^{18}O$  in precipitation ( $\delta^{18}O_p$ , ‰). Simulated preindustrial annual and seasonal average values are also provided. All values reported are greater than 95% significant (student's  $t$  test) given the control decadal variability about the 100-year mean.

**Table 3.** Comparison of Simulated Annual Average Preindustrial Site SATs (Tsite, °C), Tsource (°C), Precipitation Amount (PR, mm/day), Accumulation Rate (cm Water Equivalent/Year), Deuterium Excess in Precipitation ( $d$ , ‰), and  $\delta^{18}O$  in Precipitation ( $\delta^{18}O_p$ , ‰) With Observed Values for Each of the GRIP, NGRIP, EDC, and EDML Ice Core Sites<sup>a</sup>

|     |                  | GRIP  |        | NGRIP |        | EDC   |        | EDML  |       |
|-----|------------------|-------|--------|-------|--------|-------|--------|-------|-------|
|     |                  | Model | Obs    | Model | Obs    | Model | Obs    | Model | Obs   |
| 0k  | Tsite            | -29.9 | -31.6  | -30.4 | -31.7  | -44.0 | -54.5  | -34.3 | -44.6 |
|     | Tsource          | 10.7  | ~15-20 | 9.8   | ~16-21 | 5.4   | ~10-15 | 10.7  | ~5-10 |
|     | Accumulation     | 4.8   | 19.0   | 12.3  | 23.0   | 2.4   | 2.5    | 3.2   | 6.4   |
|     | PR               | 0.1   | 0.3    | 0.4   | 0.6    | 0.1   | 0.3    | 0.2   | 0.5   |
|     | $d$              | 11.9  | 10.5   | 12.8  | 9.5    | 6.7   | 9.3    | 9.5   | 4.7   |
|     | $\delta^{18}O_p$ | -34.7 | -35.5  | -34.9 | -35.2  | -38.2 | -50.7  | -39.3 | -44.8 |
| 21k | Tsite            | -12.2 | -21.0  | -9.7  | -9.7   | -9.2  | -8.1   | -7.4  | -7.9  |
|     | Tsource          | -2.9  | ~-6    | -4.2  | -4.2   | -1.8  | -2.9   | -3.1  | -2.7  |
|     | $d$              | -4.3  | ~-6    | -4.9  | -4.9   | -5.3  | -2.9   | -3.5  | -2.0  |
|     | $\delta^{18}O_p$ | -1.1  | ~-5    | -0.9  | -0.9   | -1.1  | -5.2   | -0.1  | 5.3   |

<sup>a</sup>Observed values for Tsite, Tsource,  $d_p$ , and  $\delta^{18}O_p$  are provided by *Stenni et al.* [2010] for EDC and EDML, and isotopic values are core top averages (~1.2–2.0 kyr BP). Present-day values for GRIP and NGRIP are taken from *Masson-Delmotte et al.* [2005b]. Simulated precipitation is compared to climate prediction centre merge analysis of precipitation reanalysis data [*Xie and Arkin*, 1996]. In addition, comparisons between simulated and reconstructed isotope and temperature values are provided for the LGM (EDC: *Stenni et al.* [2004]; GRIP: *Masson-Delmotte et al.* [2005a]; EDML: *Stenni et al.* [2010]) and anomalies are average values over the period ~20–22 kyr BP. Modeled LGM  $\Delta Tsource$  anomalies represent average SST (rather than SAT) values within the simulated source region. Comparison is not given for NGRIP, as the deuterium excess record for this site has not been interpreted quantitatively for the LGM.

notably lower than observed for the NH sites due to comparatively smaller simulated precipitation rates. Annual average simulated site temperatures are similar to observed for GRIP and NGRIP, although the warm bias over the southern high latitudes is apparent for EDC and EDML. The observed seasonal SAT cycle at each site is captured well within the model (Supplementary Figure 3), with this warm bias evident particularly during the winter months at the Antarctic sites. Agreement between simulated and observed isotopic values is closer for GRIP and NGRIP than the Antarctic sites, where simulated  $d$  is underestimated at EDC and overestimated at EDML (Table 3). Overall, the observed intersite gradients (between GRIP/NGRIP and EDC/EDML) are not captured in the preindustrial simulation. It should also be noted that the

Dome C region is described as localized and variable in terms of temperature, isotopic composition of precipitation, and accumulation rates [*Masson-Delmotte et al.*, 2008], and model resolution is important for capturing observed isotopic gradients in Antarctica [*Werner et al.*, 2001]. Hence, comparison of mean gridbox values with observational point data may not produce a close agreement. Also, snowfall deposition occurring in the form of clear sky precipitation, which is not well resolved GCMs [*Masson-Delmotte et al.*, 2008], may impact model-observational comparisons at EDC.

[30] Additional comparisons with reconstructed LGM values show that simulated Tsite changes for EDC and EDML are close to the estimates from isotopic reconstructions, although simulated Tsite and  $\delta^{18}O_p$  values at GRIP

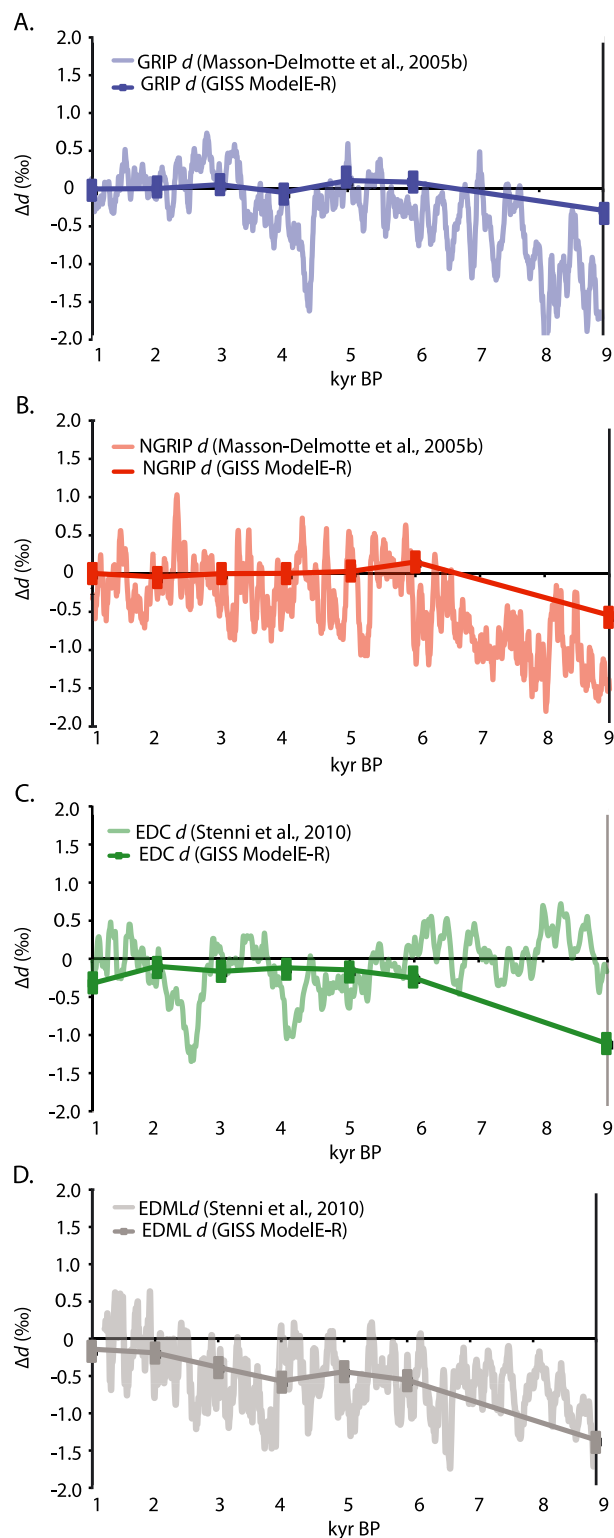


**Figure 3.** Comparison of simulated  $d$  anomalies throughout modeled Holocene time slices (1, 2, 3, 4, 5, 6, and 9 kyr BP) with reconstructed values over GRIP (a; *Masson-Delmotte et al.* [2005b]), NGRIP (b; *Masson-Delmotte et al.* [2005b]), EDC, and EDML (c and d; *Stenni et al.* [2010]). Model data points indicate the  $1\sigma$  decadal variability for the preindustrial control simulation as a measure of simulated natural variability. Estimates of analytical uncertainty of  $d$  vary, but may be up to  $\sim 0.64\text{‰}$  (*Masson-Delmotte et al.*, 2005a).

are subdued relative to proxy reconstructions (Table 3). Multiproxy approaches, including borehole reconstructions, suggest Tsite anomalies for the LGM in Greenland of greater than  $20^{\circ}\text{C}$  [*Dahl-Jensen et al.*, 1998], while only modest changes of  $\sim 10\text{--}12^{\circ}\text{C}$  are simulated here. The model is able to resolve the sign of the glacial-interglacial  $d$  variations as observed in Greenland and Antarctic ice cores, which has not been captured in previous studies using simulations forced with CLIMAP SST reconstructions [*Werner et al.*, 2001].

[31] We also compare ModelE simulated  $d$  anomalies with reconstructed changes from ice core records throughout the Holocene (Figure 3). Over the Greenland sites, modeled annual average  $d$  anomalies (relative to the control simulation) largely resemble those reconstructed from the Holocene section of the GRIP record, with an increase in  $d$  from between 9 and 6 kyr BP. The correspondence between simulated and reconstructed  $d$  values is lower over the Antarctic EDC site, with greater negative anomalies simulated in the early Holocene, compared with measured values [*Stenni et al.*, 2010], although the reconstructed  $d$  trend is simulated well for EDML.

#### 4.2. Preindustrial VSDs

[32] For GRIP and NGRIP sites, the dominant annual average control source of precipitation is located in the western North Atlantic (Figure 4), which comprises  $\sim 72\%$  of total precipitation. Regional tracers are in agreement with moisture sources diagnosed by reanalysis-based and conceptual models [*Johnsen et al.*, 1989; *Barlow et al.*, 1997; *Sodemann et al.*, 2008]. The precipitation source to NGRIP is more disperse than GRIP, and regional tracers indicate an increased fraction of moisture transported from distal sources over continental North America and the northern Pacific basin (by  $\sim 8\%$ ) and a decreased contribution from the North Atlantic (by  $\sim 14\%$ ). The increased mean vapor transport distance of simulated moisture to NGRIP of  $\sim 380$  km, compared to GRIP, supports previous studies indicating more remote precipitation sources for this site [*Masson-Delmotte et al.*, 2005b]. A greater proportion of precipitation is derived from the North Atlantic region southeast of Greenland during the boreal winter months (DJF), while during the summer (JJA), there is an increase in precipitation to Greenland sites with a Pacific Ocean evaporative source and from the high northern latitudes around Greenland. The summertime Pacific source includes a significant contribution of continentally derived recycled moisture from North America ( $\sim 50\%$ ).

[33] Over Antarctica, the mean source of simulated annual control precipitation to EDML is located at  $\sim 42^{\circ}\text{S}$ , with the majority of moisture sourced from the South Atlantic and Southern oceans (Figure 4). There is also a contribution of long-distance moisture transport to this site from the mid-latitude Pacific in agreement with Lagrangian back trajectories analyses at ice core sites [*Sodemann and Stohl*, 2009]. Supporting seasonal observations [*Masson-Delmotte et al.*, 2008], there is a greater proportion of modeled moisture to EDML with a provenance in the South Atlantic during the austral winter months (JJA) and a greater amount of continentally recycled moisture during the summer months (DJF), when regional evaporative rates are higher. Over EDC, the simulated annual control precipitation

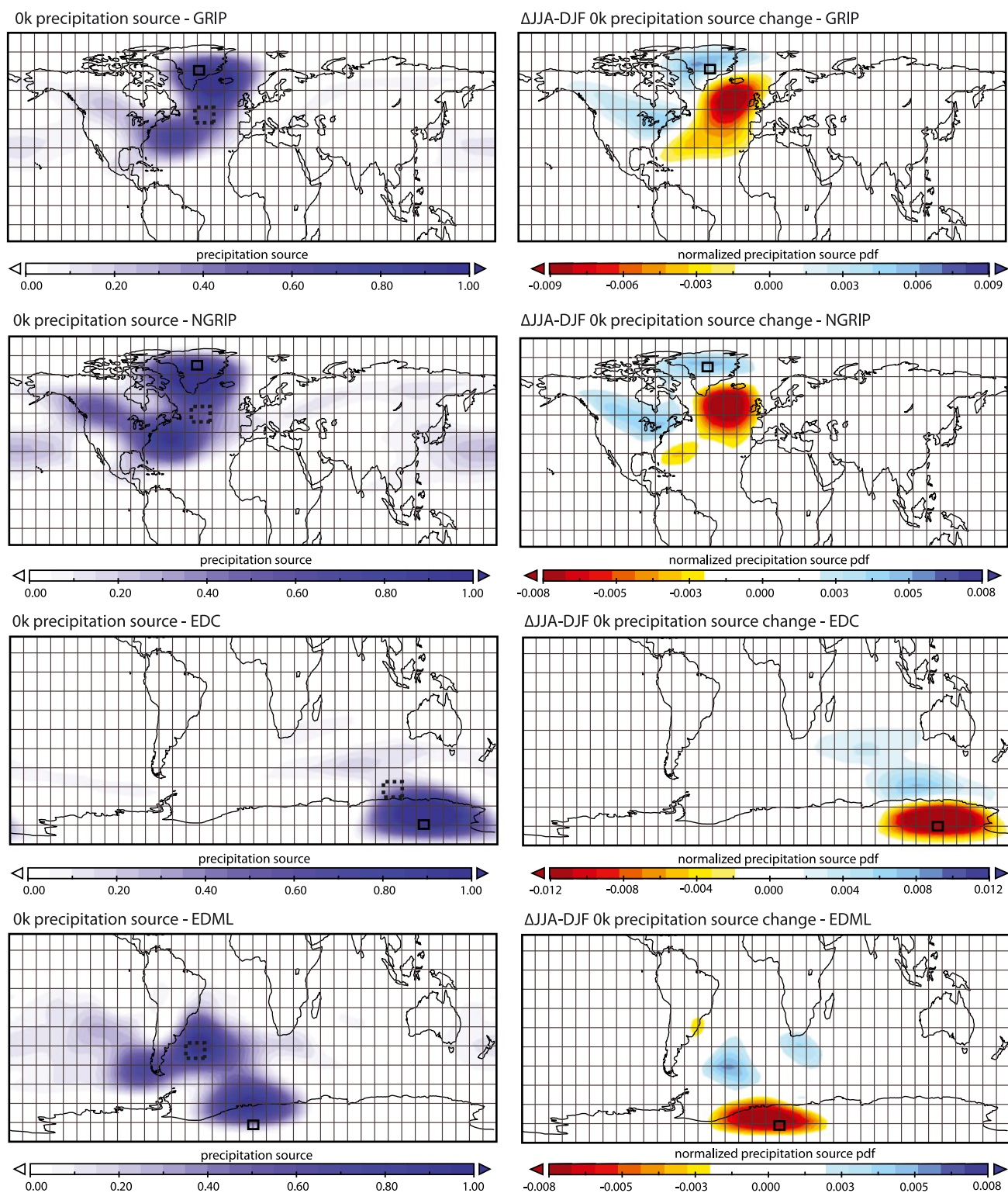


**Figure 4.** Simulated control precipitation source distributions (0k, left) and seasonal precipitation source region anomalies (JJA/DJF, right) for Greenland sites GRIP and NGRIP and Antarctic sites EDC and EDML. Solid black rectangular boxes indicate the ice core sites (end member precipitation), and dashed boxes indicate the mean location of the precipitation source region to each site. Precipitation source distributions are unitless probability density functions normalized by the maximum probability density.

(mean location  $\sim 58^{\circ}\text{S}$ ) consists of locally sourced moisture dominated by the Southern Ocean within the Indian Ocean basin and recycled moisture from continental Antarctica. A

summer-dominated snowfall regime at EDC is modeled with a significant recycled component. During the austral winter months, the main source of precipitation is comparatively

distal ( $\Delta TD \sim 2800$  km), located within the Southern and southern Indian oceans ( $\sim 60\%$  from regional tracers). Previous studies suggest the main source of EDC precipitation is located in the mid-latitude Indian Ocean, with a more southward EDML moisture source region within the South Atlantic Ocean [Stenni *et al.*, 2010]. However, simulated VSDs do not support a more southward source for EDML relative to EDC. Observational studies characterize EDC climates as highly localized [Bromwich *et al.*, 2004], and distinct moisture source regimes are inferred for high- (EDC) and low-elevation (EDML) sites, with low-elevation sites more influenced by higher-latitude moisture while high-elevation sites are more influenced by lower-latitude moisture [Masson-Delmotte *et al.*, 2011].

[34] Sublimation sources are an important component of Antarctic snowfall, with mass balance estimates suggesting sublimation effects of up to 40% in coastal locations [Bromwich *et al.*, 2004]. At EDC, however, the overestimation of recycled precipitation sources is likely, with back-trajectory analyses also indicating a lower-latitude moisture source for this site [Sodemann and Stohl, 2009]. Previous studies note that GCMs can overestimate the importance of recycling in the hydrological cycle, compared with advective moisture sources [Ruiz-Barradas and Nigam, 2006], which may have implications for the isotopic composition of snowfall [Masson-Delmotte *et al.*, 2011]. The overestimation of recycling at EDC may result from the warm bias at this continental site, although it is not considered prohibitive to comparing synthetically derived source temperature estimates with simulated VSD temperature values, as only climatological anomalies relative to the preindustrial are considered here.

### 4.3. VSD Changes

[35] Both VSD and regional water tracers show changes in source regions to the four ice core sites throughout the suite of simulations (Figures 5 and 6). During the mid-Holocene experiment, there is only a small simulated northward shift (relative to preindustrial) in the mean precipitation source to GRIP of  $\sim 1^\circ$  in latitude that corresponds to a  $\sim 100$  km decrease in vapor TD. For NGRIP, there is a similar northward source shift, together with a decrease in mean vapor TD, of  $\sim 145$  km during the mid-Holocene. Additionally, there is an increase in Pacific-sourced moisture to this site during this time slice (of  $\sim 6\%$ ) and a concomitant decrease in the contribution of moisture originating in the Atlantic. Over Antarctica, a mid-Holocene southward source shift is modeled at EDML ( $\sim 2^\circ \Delta lat$ ,  $\Delta TD \sim 180$  km), although the latitudinal change at EDC is comparatively smaller ( $\sim 0.5^\circ \Delta lat$ ,  $\Delta TD \sim 320$  km). In both high-latitude regions, there are minimal corresponding changes in precipitation amount during the mid-Holocene.

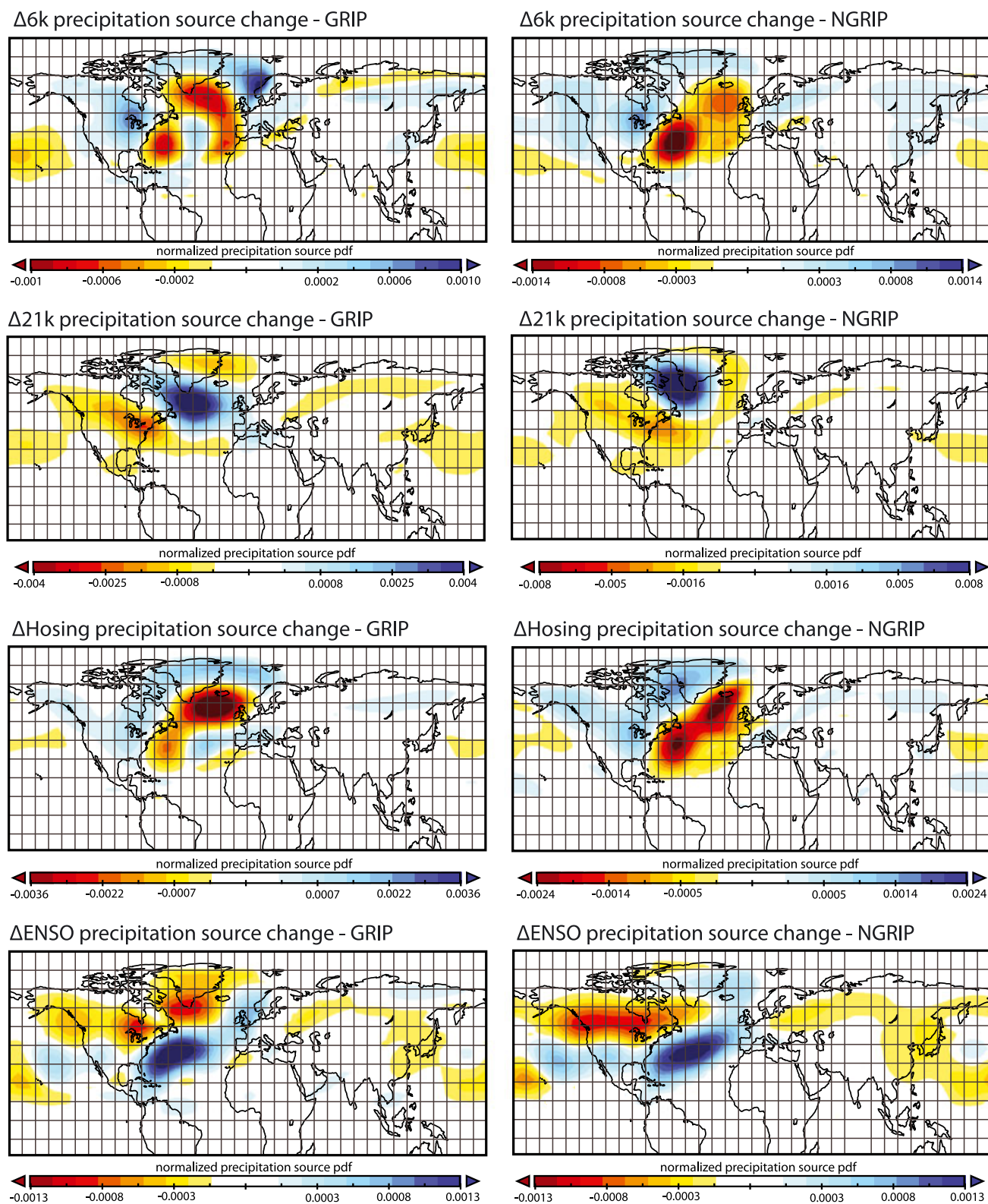
[36] During the 21k experiment, VSD tracers indicate minimal mean source location changes for GRIP, with complex spatial VSD changes occurring (Figure 5). A larger mean northward source change (of  $\sim 7^\circ$  in latitude) is simulated at NGRIP, compared with the preindustrial simulation. During the LGM, both sites' regional tracers show an increased fraction of North Atlantic precipitation (GRIP  $\sim 11\%$ ; NGRIP  $\sim 18\%$ ), with simulated decreases in mean vapor TD to these Greenland sites of up to 800 km; simulated moisture sources are more localized during the LGM.

These changes are also associated with a decrease at both sites in the amount of precipitation that is greatest in the summertime (GRIP JJA  $\sim 30\%$ ; NGRIP JJA  $\sim 20\%$ ). Simulated SST anomalies for the LGM, relative to the preindustrial, are similar to synthesized proxy reconstructions [MARGO Project Members, 2009] around the oceanic source regions to the northern ice core sites (Figure 7), although interpretations of proxy reconstructions indicate a southward moisture source shift to GRIP of  $\sim 5^\circ$  in latitude during the LGM. Prior model studies assign variable source region changes to Greenland during the LGM under prescribed SSTs [Werner *et al.*, 2001; Langen and Vinther, 2009]. The simulated reduction in the North American source with the addition of the Laurentide at the LGM (by  $\sim 5\%$ ) is also observed in sensitivity experiments [Langen and Vinther, 2009; MARGO Project Members, 2009].

[37] Over Antarctica, there are also decreases in precipitation amount during the LGM at both sites (EDC ANN  $\sim 60\%$ ; EDML ANN  $\sim 55\%$ ). The shift in mean source region location for the 21k simulation is substantial at both sites (EDC  $\sim 3^\circ \Delta lat$ ,  $\sim 13^\circ \Delta long$ ; EDML  $\sim 4^\circ \Delta lat$ ,  $\sim 2^\circ \Delta long$ ) and predominantly southwestward. This is associated with decreases in vapor transport distances (EDC  $\Delta TD \sim 640$  km; EDML  $\Delta TD \sim 470$  km), a greater contribution to both sites from the Southern Ocean region, and a reduced mid- and low-latitude moisture component. Previous GCM results indicate that LGM source region shifts for Atlantic-influenced Antarctic regions are minimal, while Pacific-dominated source changes are greater [Werner *et al.*, 2001]. Although the strong expansion of LGM sea ice was highly seasonal [Gersonde *et al.*, 2005], the southward LGM source shift for EDC again results in an overly significant contribution of sublimated snowfall ( $\sim 60\%$ ) to this site during summer for this time slice. Considering the oceanic component of the EDC source only, the shift at the LGM is significantly westward.

[38] Regional tracers in the freshwater-forced experiment reveal increases of up to  $\sim 15\%$  in the contribution of the North Atlantic to total annual precipitation at NGRIP and GRIP. This is associated with an overall decrease in precipitation to these sites ( $\sim 0.1$  mm/day), including a decrease in moisture advected to Greenland from the Pacific. Overall, the mean TD of vapor to GRIP is unchanged. Following freshwater injection, moisture transport distance to NGRIP is reduced by  $\sim 134$  km, compared with during the preindustrial. For the EDML Antarctic ice core site, freshwater forcing results in a source shift close to the site ( $\sim 3^\circ \Delta lat$ ) and a corresponding decrease in mean moisture TD of  $\sim 370$  km, although there is no significant change in the overall amount of precipitation to the Antarctic sites following freshwater injection. The Southern Ocean dominates the freshwater-forced source to EDML, with a decrease in moisture transported from the southern Atlantic. At the EDC site, the freshwater-forced source is largely stationary relative to the present day, with a small westward shift in mean source location by  $\sim 2^\circ$ .

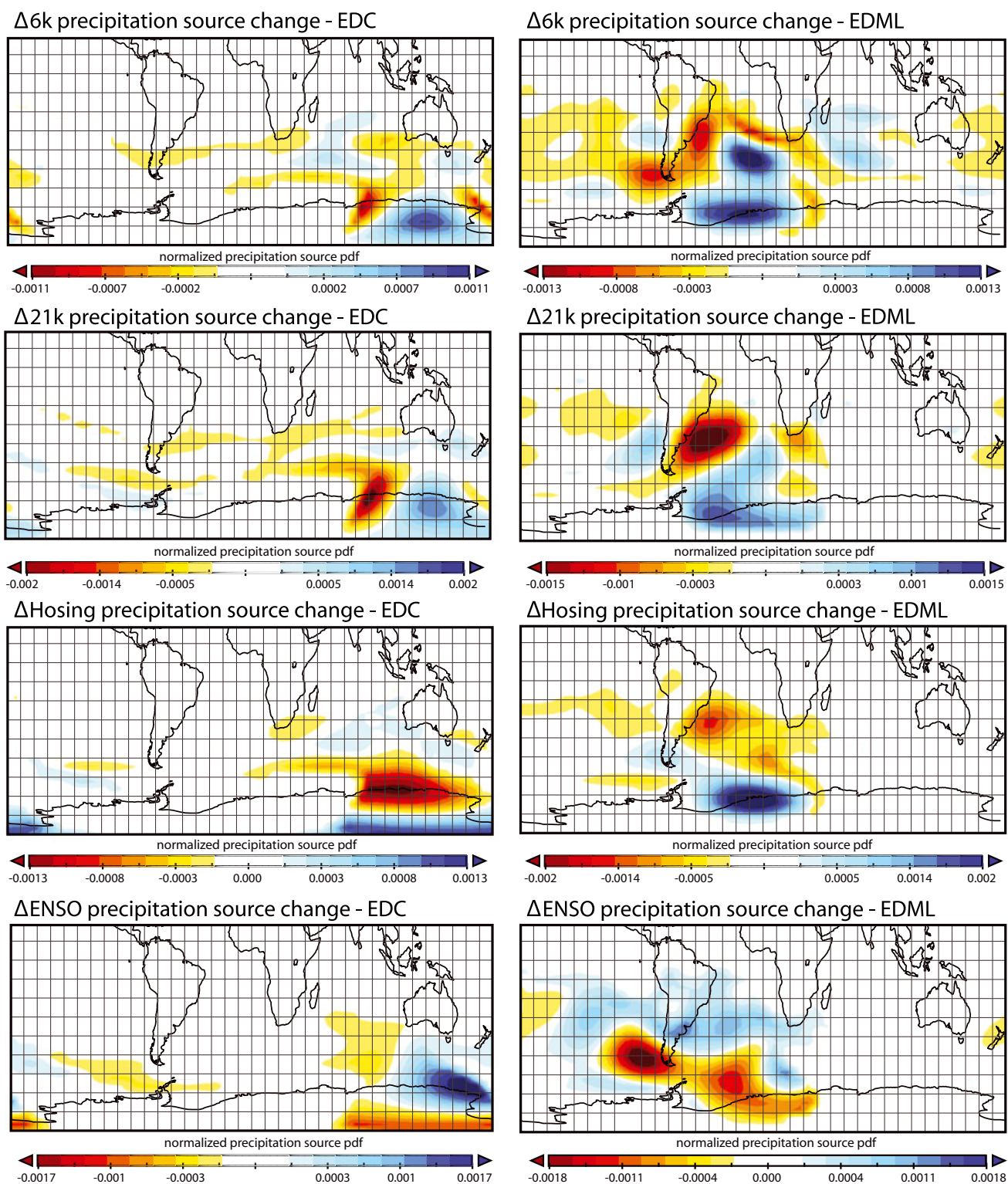
[39] For the ENSO-type experiments, the ENSO+ phases are associated with increases in annual average precipitation at all sites. For GRIP, there is a southward source shift of  $\sim 1.5^\circ$  and an increase in TD of  $\sim 170$  km. During simulated positive ENSO phases, there is a decrease in both



**Figure 5.** Simulated precipitation source distribution anomalies for GRIP (left) and NGRIP (right) sites for the 6k, 21k, freshwater-forced (hosing), and ENSO-like experiments. Precipitation source distributions are unitless probability density functions normalized by the maximum probability density. Site locations are indicated in Figure 4.

Pacific-sourced vapor and moisture from the Labrador Sea to this site. The largest GRIP source increase for the ENSO+ experiment occurs from the mid-latitudes of the Atlantic.

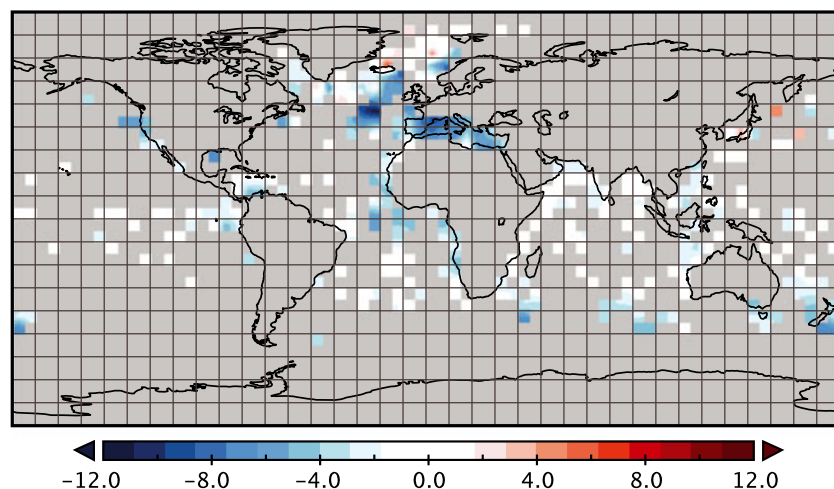
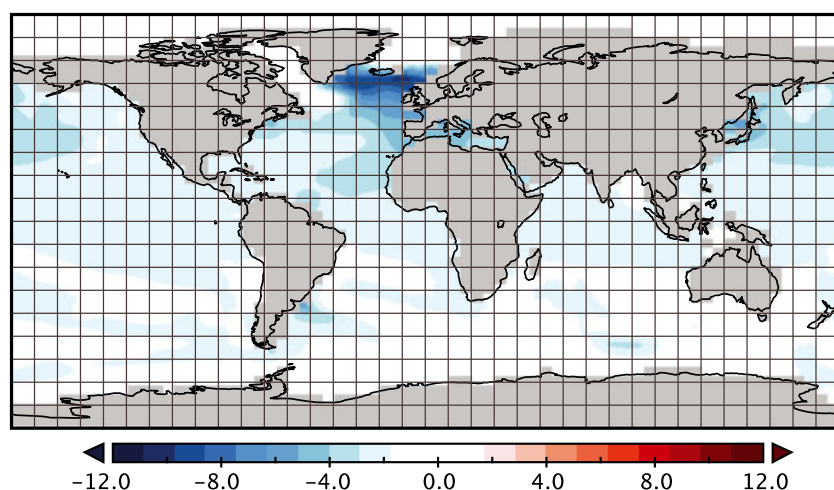
A similar fingerprint of ENSO phases is modeled for the moisture source to NGRIP. For the Antarctic sites, the largest ENSO simulation impacts occur for the EDML,



**Figure 6.** Simulated precipitation source distribution anomalies for EDC (left) and EDML (right) sites for the 6k, 21k, freshwater-forced (hosing), and ENSO-like experiments. Precipitation source distributions are unitless probability density functions normalized by the maximum probability density. Site locations are indicated in Figure 4.

which has a stronger Pacific precipitation influence than EDC (~25% of total annual precipitation from the Pacific for EDML, ~8% for EDC from regional tracers). There is a shift in mean precipitation ( $\sim 2^\circ$   $\Delta$ lat,  $\sim 4.5^\circ$   $\Delta$ long) and

increase in mean vapor TD by  $\sim 550$  km, associated with positive ENSO phases at this site. At EDC, there is an eastward shift in mean source by  $\sim 5^\circ$  and a decrease in transport distance by  $\sim 150$  km.

A. MARGO  $\Delta$ LGM SST ( $^{\circ}$ C)B. GISS ModelE-R  $\Delta$ LGM SST ( $^{\circ}$ C)

**Figure 7.** (a) Proxy-derived MARGO synthesis SST anomalies (SST,  $^{\circ}$ C) (*MARGO Project Members, 2009*) for the LGM and (b) equivalent SST anomalies for the ICE-5.2G-LIC experiment using the GISS ModelE-R.

#### 4.4. Source Region Characteristics

[40] Assessment of the accuracy of simulated average source region temperature changes for the core sites is limited, as there are few periods detailed in proxy studies that are characterized by significant  $d$  and source temperature change. We consider the LGM the most useful basis for model-proxy data comparison of source temperatures, as this period is significantly different climatically from the preindustrial and boundary conditions are comparatively well known. Generally, simulated patterns of LGM SST anomalies are reasonably close to proxy-derived reconstructed values (Figure 7). At the GRIP site, the modeled LGM source SAT change of  $\sim 7^{\circ}$ C is close to the  $\sim 6^{\circ}$ C reconstructed from coisotopic approaches [*Masson-Delmotte et al., 2005a*]. Over Antarctica, the simulated LGM source temperature change to EDC ( $\sim 7^{\circ}$ C) is greater than the  $\sim 3^{\circ}$ C suggested by proxy reconstructions [*Stenni et al., 2010*], although the modeled site temperature change of  $\sim 9.2^{\circ}$ C is in good agreement with reconstructed changes of  $\sim 8^{\circ}$ C. The offset between simulated and reconstructed

LGM source temperature changes at EDC may relate to the discrepancy in the proposed location of source regions to this site and particularly to the likely simulated overestimation of land-derived snowfall.

#### 5. Evaluation of $d$ as a Tracer of Source Temperatures

[41] For each ice core site (GRIP, NGRIP, EDC, and EDML), average modeled  $\Delta T_{\text{source}}$  values determined using VSD tracers are compared to synthetic  $\Delta T_{\text{source}}$  values derived from equations (2) and (3) for annual and seasonal (JJA, DJF) average changes for each simulation (Figure 8). Similarly, a comparison is made between modeled synthetic  $\Delta d$  values (Figure 8). Most modeled VSD average source temperature data points match synthetically derived equivalents well, particularly given that the uncertainty of the isotopic inversion (equations (2) and (3)) method is  $\sim 2\text{--}3^{\circ}$ C on  $\Delta T_{\text{source}}$  and  $\Delta T_{\text{site}}$  reconstructions [*Masson-Delmotte et al., 2005a*].

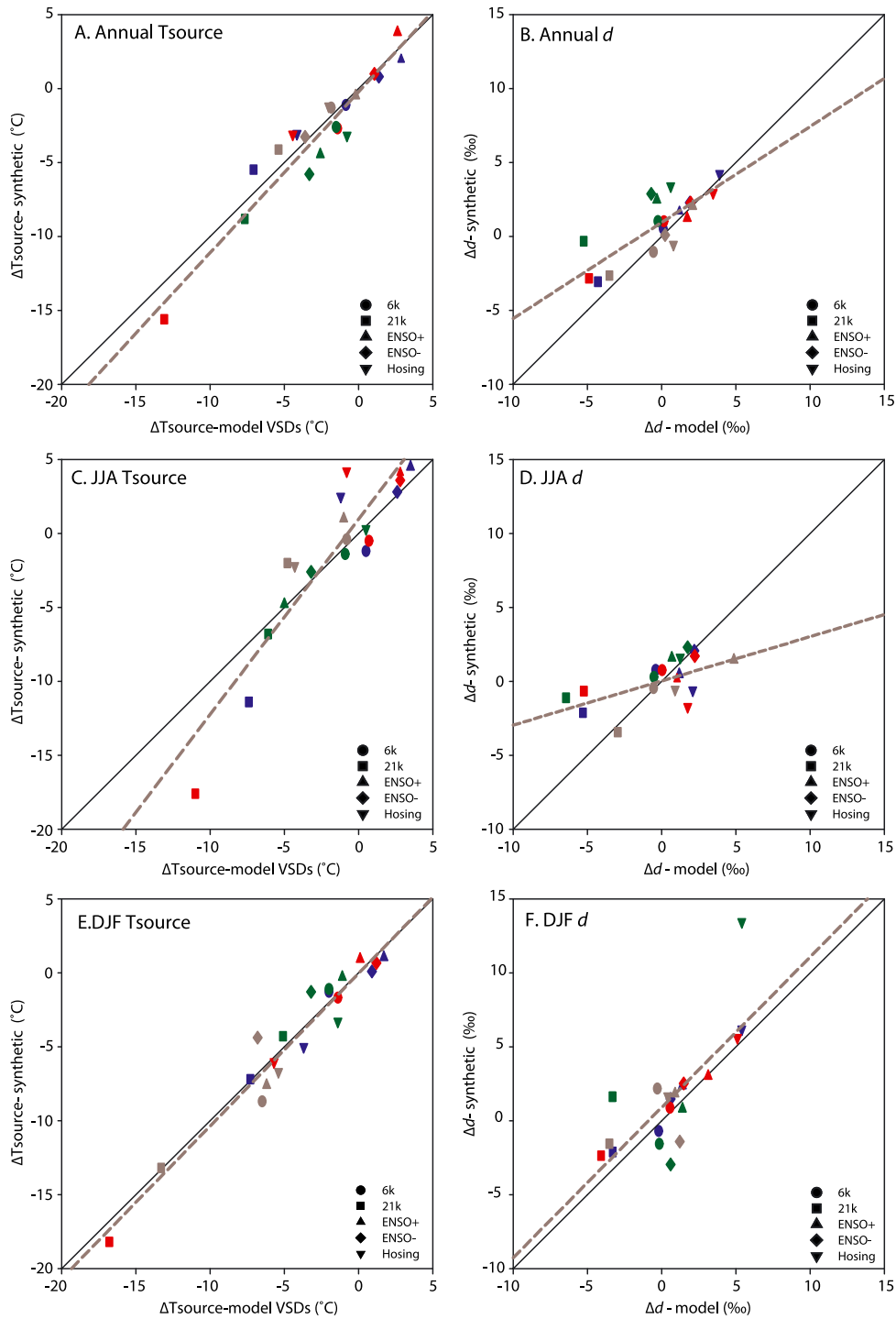


**Figure 8.** Comparison of synthetic and model VSD  $\Delta T_{\text{source}}$  (panels a, c, and e) and model  $\Delta d$  (panels b, d, and f) estimates for 6k, 21k, freshwater-forced (hosing), ENSO+, and ENSO- experiments for GRIP (blue), NGRIP (red), EDC (green), and EDML (grey) ice core sites. Comparisons are made for annual, JJA, and DJF averages. Simulated  $T_{\text{source}}$  values are determined using average values within modeled VSD regions, and model  $d$  values are determined as climatological values within the relevant ice core gridbox. Synthetic  $T_{\text{source}}$  and  $d$  values are calculated from empirical relationships (Stenni *et al.*, 2001; Masson-Delmotte *et al.*, 2005a) using modeled  $T_{\text{site}}$  and  $\delta^{18}\text{O}_{\text{sw}}$  fields. The solid line indicates the 1:1 relationship between the  $T_{\text{source}}$  or  $d$  changes, where estimates from both techniques are identical. The dashed gray line indicates the line of best fit for each panel.

### 5.1. Greenland Sites

[42] For the mid-Holocene and ENSO-like experiments, a close agreement occurs between  $\Delta d$  and  $\Delta T_{\text{source}}$  estimates from modeled and synthetic values, indicating that  $d$  is generally a faithful tracer of source region temperatures for Greenland under these boundary conditions. We identify the largest discrepancies in  $\Delta d$  and  $\Delta T_{\text{source}}$  comparisons using these two techniques for the LGM simulation, particularly during the boreal summer. Discrepancies could indicate multiple climatic influences on  $d$  during this time, or that deficiencies exist in either MCIM-derived  $d$ - $T_{\text{source}}$  relationships or the GCM experiments.

[43] The LGM was characterized by marked topographic changes within the cryosphere [Clark *et al.*, 2009]. High-latitude regions are sensitive to changes in boundary conditions associated with the glacial augmentation of the ice sheets and sea-ice extent, such that glacial atmospheric circulation was significantly altered [Jouzel *et al.*, 1982]. Furthermore, Greenland precipitation is a heterogeneous and dynamic mix of moisture sources with different distillation histories [Charles *et al.*, 1994] and is responsive to regional perturbations in circulation patterns. During the LGM, the blocking of low-level atmospheric flow by topography (principally the Laurentide Ice Sheet) impacted polar front and regional cyclogenesis and advection of moisture into central Greenland was significantly perturbed [Werner *et al.*, 2000; Langen and Vinther, 2009]. Simulated glacial changes in the region include an increase in eastward near-surface airflow around Greenland, a simulated southward deflection of atmospheric jets, and a strengthening of the polar front in response to orographic forcing (Figure 9). The steering influence of the Laurentide Ice Sheet on regional circulation also affects the moisture source and

isotopic composition of precipitation throughout the Arctic region. Moisture is advected on transport pathways of significantly different lengths and temperature profiles, which impacts the retention of heavy isotopes in vapor and the composition of end-member precipitation. Regional tracers indicate that during the LGM there was an annual average decrease in Pacific-sourced moisture ( $\sim 15\%$ ) from the preindustrial contribution of  $\sim 24\%$  (Figure 9). This is consistent with the reduction of the Pacific source under the influence of the Laurentide determined from previous model experiments [Charles *et al.*, 1994].

[44] The largest discrepancies in  $\Delta T_{\text{source}}$  comparisons for Greenland sites occur during the boreal summer months. The importance of the seasonal intermittency of precipitation for isotopic variability over high-latitude sites is well noted, although poorly constrained for LGM climates [Masson-Delmotte *et al.*, 2005a, 2008]. Glacial conditions inhibit winter snowfall due to both circulation changes in response to the Laurentide Ice Sheet and altered thermal oceanic gradients. Simulated dry glacial winters may result from a shift toward more zonal circulation patterns that preclude onshore advection to Greenland and reduce the contribution of strongly isotopically depleted precipitation to the annual total [Jouzel *et al.*, 2007]. In addition, there is a substantial increase in the continentality of central Greenland during the LGM [Otto-Bliesner *et al.*, 2007; MARGO Project Members, 2009]. This includes a simulated  $4\text{--}8^\circ$  ( $1\text{--}2$  gridbox) latitudinal LGM expansion southward of sea ice in the North Atlantic in the wintertime and an annual average simulated increase in NH horizontal snow and sea-ice coverage of  $\sim 10\%$ . Simulated LGM winter precipitation comprises less than 15% of the annual total to GRIP and NGRIP, and the seasonal cycle of precipitation is accentuated at this time relative to the control simulation.

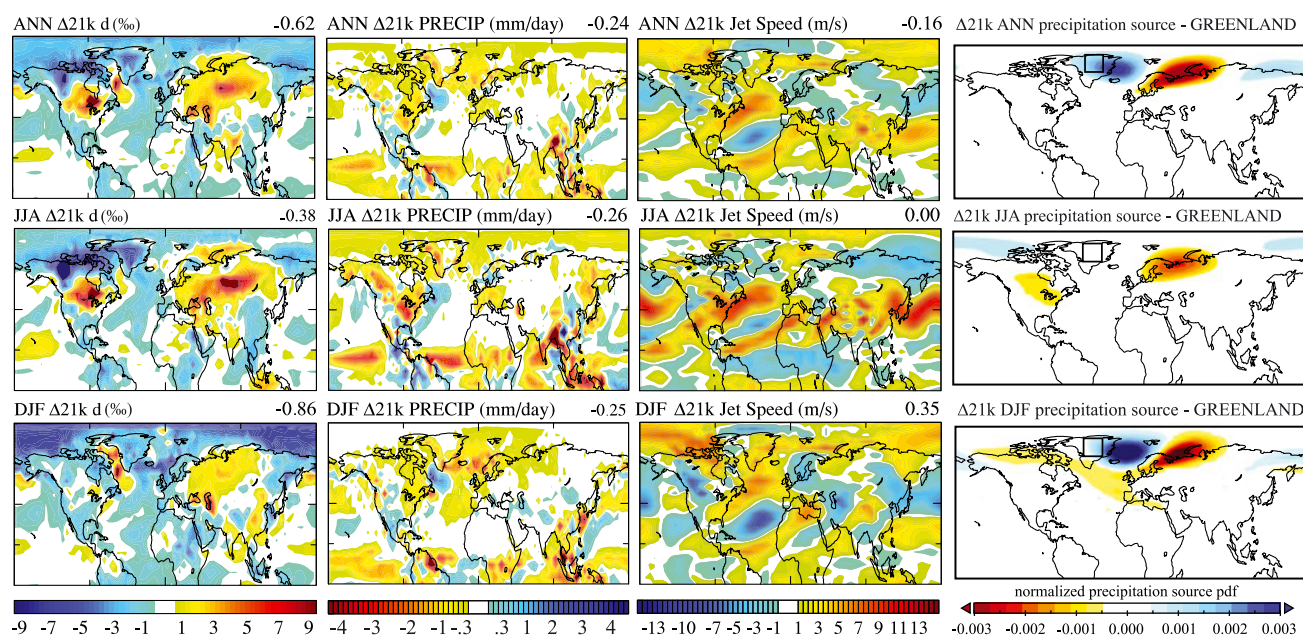


**Figure 9.** Simulated LGM annual (ANN) and seasonal (JJA, DJF)  $d$  (‰, left) and precipitation (mm/day, middle left) and jet speed (m/s, middle right) anomalies and Greenland precipitation source region anomalies (right). VSDs are unitless probability density functions normalized by the maximum probability density. The Greenland region ( $70\text{--}80^\circ\text{N}$ ,  $35\text{--}45^\circ\text{W}$ ) encompasses both GRIP and NGRIP ice core sites.

[45] During summer under preindustrial conditions, the evaporative source to the Greenland ice core site lies predominantly in the Pacific Ocean and high latitudes around Greenland, and these sources are strongly perturbed by changes in the regional LGM topography (Figure 9), including the expanded summer sea-ice extent. For example, there is a ~25% increase in the contribution of the North Atlantic source to GRIP summer precipitation during the LGM. *Masson-Delmotte et al.* [2005a] note that the application of isotopic inversions without accounting for precipitation seasonality biases produces unrealistic  $\Delta T_{\text{source}}$  estimates, and hence the significant LGM changes in the seasonality of both precipitation regimes and source region locations for the Greenland sites may result in  $T_{\text{source}}$  discrepancies between simulated and synthetic estimates. In this instance, the comparison attempted here may benefit from seasonally specific regression coefficients.

[46] Given the sensitivity of regional climates to topography, the accurate parameterization of ice-sheet orography is critical for accurately capturing the character of NH atmospheric circulation, precipitation [Kageyama and Valdes, 2000], sea-ice extent, and meridional temperature gradients [*Masson-Delmotte et al.*, 2005a]. Therefore, a second comparison of  $\Delta T_{\text{source}}$  estimates using the VSD tracers and numerical relationships was also made for the second LGM experiment that was run with standard ICE-5.2G boundary conditions (see Table 1; *Peltier* [2004]). The correspondence of LGM ICE-5.2G  $T_{\text{source}}$  changes for the two techniques is significantly lower than for the modified Laurentide equivalent (average Greenland 5.2G-LIC  $T_{\text{source}}$   $R^2 = 0.7$ ; 5.2G  $T_{\text{source}}$   $R^2 = 0.2$ ). This difference highlights the importance of topography on regional hydrology and indicates that  $\Delta T_{\text{source}}$  and  $d$  estimate offsets may be an artefact of poor model ice-sheet representation. It is possible that in this topographically sensitive experiment, the model resolution and prescribed LGM boundary conditions utilized here may be inadequate to resolve topography critical for regional climatologies, and a higher-resolution model incorporating ice-sheet dynamics, such as horizontal advection, may improve the simulation of regional LGM climatologies [*Carlson et al.*, 2008] and the comparison of  $\Delta T_{\text{source}}$  estimates. However, it should be noted that the correct sign of LGM present-day  $d$  anomalies is captured in the simulations utilized here, whereas in previous atmospheric LGM simulations forced LGM forced with CLIMAP SSTs, erroneous  $d$  anomalies in Greenland occurred [e.g., *Werner et al.*, 2001].

[47] Overall, comparison of  $T_{\text{source}}$  estimates at these Greenland sites suggests that deuterium excess may poorly record source temperature conditions in some instances by the proposed empirical scalings (equations (2) and (3); *Stenni et al.* [2001]; *Masson-Delmotte et al.* [2005a]), particularly where boundary conditions are substantially different. As certain aspects of simulated LGM hydrology over Greenland (e.g.,  $\Delta d_p$  over GRIP and VSD-derived  $\Delta T_{\text{source}}$ ) do correspond closely with reconstructed proxy records, it may be that simplifications in numerical  $d$ - $T_{\text{source}}$  primarily contribute to offsets between the  $\Delta T_{\text{source}}$  estimates for the LGM. For example, the pronounced LGM seasonality changes may affect the applicability of numerical regressions (equations (2) and (3)) in the manner attempted here, as these are valid for individual precipitation events, but do not take into account seasonality changes in either snowfall or the isotopic composition of precipitation [*Jouzel et al.*, 2007]. The assumption of

temporal invariance in seasonality is known to result in erroneous site temperature estimates from isotopic profiles from Greenland and seasonal corrections have been required previously [*Masson-Delmotte et al.*, 2005b]. Although the isotope inversion models have been applied at glacial-interglacial timescales, their validity for boundary conditions very different from the present remains to be demonstrated, and in these cases, unique inversions may be necessary [*Uemura et al.*, 2012].

## 5.2. Antarctic Sites

[48] For EDML,  $T_{\text{source}}$  and  $d$  changes are similar for modeled and synthetic estimates (Figure 8), indicating that deuterium excess may provide a robust proxy for moisture source temperatures in different climatic states. Conversely, larger disparities occur at EDC, the higher-elevation Antarctic site, particularly for the LGM and summer freshwater-forced comparisons. Synthetic and simulated EDC  $\Delta T_{\text{source}}$  estimates are similar, although corresponding  $\Delta d$  comparisons are comparatively poorer. Comparisons for the EDC site may be susceptible to poor simulation of snowfall regimes due to a simulated warm continental bias and an overestimation of moisture recycling from the continent. Simulated preindustrial  $d_p$  is, for example, enriched relative to observed values in this region (Table 2). In this region,  $d$  is particularly topographically dependent, and model-observation mismatches may result from inaccuracies in representations of both cloud microphysics and water-vapor advection (*Masson-Delmotte et al.*, 2008). Discrepancies in  $T_{\text{source}}$  and  $d$  estimates suggest that this site is indeed susceptible to local or regional-scale model shortcomings.

[49] Although  $\Delta d$  offsets are seasonally robust for EDC and largely ubiquitous across the suite of simulations, the largest discrepancies occur at the colder end of the climate spectrum (i.e., the LGM and freshwater-forcing experiments). As such, inadequacies in simulated climatological regimes at this site (such as the noted warm bias) may be exacerbated during these extreme cold times. For example,  $d$  variability depends on microphysical processes prevailing in clouds, including kinetic fractionation, during the processes of condensate formation from atmospheric vapor [*Jouzel and Merlivat*, 1984], which are variable under differing climate states. For snow formation occurring in a supersaturated environment, such as over ice, a kinetic fractionation effect transpires similar to that existing during evaporation (*Jouzel et al.*, 1982, 1991) and depends on highly local supersaturation conditions when condensing water vapor to ice [*Schmidt et al.*, 2005]. For a given deuterium excess in vapor, the effect of ice condensation from atmospheric vapor is to lower  $d$  values in snow, although this is also temperature dependent (*Luz et al.*, 2009). The impact of condensation processes during snow formation is significant, particularly at the cold end of the climatic spectrum, and on the order of several per million (*Luz et al.*, 2009).

[50] Over Antarctica, where  $\Delta T_{\text{source}}$  estimates correspond more closely with each other than over Greenland, the impact of cold climate conditions in Antarctica is considerably more subdued. There are minimal changes in the seasonality of simulated LGM precipitation over Antarctica, which largely maintains its geographical symmetry during glacial conditions. Prior model studies indicate the effect of seasonality is of minor regional importance on glacial precipitation regimes

[Jouzel *et al.*, 2003; Stenni *et al.*, 2010]. Previously, Antarctic  $d$  variability has been considered amenable to simpler interpretations than for Greenland [Jouzel *et al.*, 2003]. In this study, the qualitative correspondence of source temperature and  $d$  values is closer for EDML than at other sites and this isotope-temperature relationship appears robust to changes in boundary conditions.

## 6. Discussion

[51] In this study, we examined changes in the SAT of the evaporative source to various locations, while reconstructions using ice core coisotopic variability generally interpret fluctuations in terms of source SST changes. Although SSTs are considered generally equivalent to SATs near the ocean surface in observational isotope analyses [Uemura *et al.*, 2008], significant SST-SAT offsets (up to  $\sim 4.5^\circ\text{C}$  during the 21k and freshwater-forced experiments) occur in modeled source regions using VSD tracers. Studies based on climate reanalyses show that although there is a close SST-SAT correlation in most regions, this relationship degrades significantly in the high latitudes, where the difference in air-sea temperatures is influenced by multiple variables, such as wind speed, surface heat fluxes, and net solar radiation [Cayan, 1992; Kara *et al.*, 2007]. In cases where source air-sea temperature differences are large, for example, changes in humidity and latent heat fluxes at the evaporative surface may also be significant, with larger air-sea temperature contrasts causing higher heat fluxes [Song and Yu, 2012].

[52] Indeed, there is a degraded correspondence of  $d$ - $\Delta T_{\text{source}}$  values when SST, rather than SAT, source averages are used for comparison between model and synthetic estimates (Table 4). Average source SAT values, when compared with SSTs, integrate a larger combination of influences on the isotopic composition of vapor during evaporative processes. Additionally, recycled moisture originating from land, rather than oceanic, sources is an important component of precipitation to proxy sites, including those in the high latitudes, and also influences the composition of water vapor. Disregarding this moisture component by investigating source SSTs, rather than SATs, neglects a significant contribution to air-mass histories.

[53] Source region characteristics that control evaporation kinetics, such as relative humidity and wind speed, also provide important climatic influences on isotopic composition [Merlivat and Jouzel, 1979]. For example,  $d$  correlates with both relative humidity at the ocean surface and with source temperatures [Uemura *et al.*, 2008] In this study,

we model significant changes in relative humidity between simulations and a seasonally dependent correspondence between  $d$  and relative humidity changes at the Greenland sites (Table 4). There are average relative humidity changes of  $\sim 25\%$  within the Greenland area precipitation source region during the LGM (Figure 9) and smaller simulated LGM anomalies ( $\sim 3$ – $9\%$ ) for the Antarctic sites. Notably, simulated Greenland source humidity differences during the LGM (Figure 9) are an order of magnitude greater than source relative humidity changes accounted for in  $T_{\text{source}}-d$  equations (2) and (3) and may introduce errors in numerical-based reconstructions. The exclusion of the influence of humidity changes in MCIM regressions may be a significant limitation of quantifying source temperature changes from isotopic profiles.

[54] Additionally, the geographical location of the evaporative source relative to the site is an important influence on the isotopic composition of end-member precipitation, as the proximity of the moisture source impacts the degree of air-mass mixing and rainout incurred *en route* to the proxy site [Charles *et al.*, 1994]. Evaporative source regions are found to be dynamic and there are significant simulated transport distance reductions from source to site between the preindustrial and LGM simulations (of up to  $\sim 800$  km), which may influence the isotopic composition of end-member precipitation, as moisture is advected on different pathways and sustains a varying degree of replenishment by other moisture sources. Deuterium excess is dependent on advection height—lower  $d$  values transpire in near-surface flow originating from localized high-latitude evaporative sources and higher-moisture transport pathways reflect more distal transport [Stenni *et al.*, 2001; Masson-Delmotte *et al.*, 2008].

[55] Generally, deuterium excess variability is associated with changes in multiple climate parameters and the relative importance of these is both regionally dependent and susceptible to changes in prescribed boundary conditions. We find that simulated Greenland hydrological regimes are sensitive to varying boundary conditions. Given the similarity of simulated and synthetic  $\Delta T_{\text{source}}$  estimates for the 6k, freshwater-forcing, and ENSO-like simulations, it may be that beyond a certain climatic threshold (i.e., during the LGM), multiple climatic influences should ideally be considered in interpreting  $d$  variability. The simplifications incorporated into the numerical inversions (equations (2) and (3)), particularly that the seasonality of precipitation is temporally static and that the source relative humidity is largely invariant, may introduce a bias into isotope-climate relationships. These considerations may ultimately result in the offset between synthetic and modeled  $\Delta T_{\text{source}}$  values over Greenland during the LGM.

**Table 4.** Correlation Coefficients (R) for GRIP, NGRIP, EDC, and EDML Site  $d$  and Simulated Source Region Average SATs and SSTs and Relative Humidity for Annual (ANN) and Seasonal (JJA, DJF) Values Correlation Coefficients Were Determined From Modeled Values Across the Suite of Simulations

| Site  | $d$ - $T_{\text{source}}$ (SAT) R |     |     | $d$ - $T_{\text{source}}$ (SST) R |     |     | $d$ - Relative humidity R |     |      |
|-------|-----------------------------------|-----|-----|-----------------------------------|-----|-----|---------------------------|-----|------|
|       | ANN                               | JJA | DJF | ANN                               | JJA | DJF | ANN                       | JJA | DJF  |
| GRIP  | 0.4                               | 0.8 | 0.0 | 0.2                               | 0.3 | 0.0 | 0.0                       | 0.1 | -0.2 |
| NGRIP | 0.6                               | 0.8 | 0.2 | 0.2                               | 0.3 | 0.1 | -0.1                      | 0.1 | -0.3 |
| EDC   | 0.6                               | 0.5 | 0.7 | 0.3                               | 0.4 | 0.2 | 0.1                       | 0.1 | 0.1  |
| EDML  | 0.7                               | 0.6 | 0.7 | 0.6                               | 0.6 | 0.5 | 0.3                       | 0.3 | 0.1  |

### 6.1. Limitations of the Study

[56] There are limitations to this study that preclude the deuterium excess from being fully assessed as a moisture source tracer under different climatic states. First, the simplifications inherent in the numerical equations (2) and (3) mean that several important climatic parameters are not explicitly represented. The regression coefficients are regionally specific, but are determined over a range of climatic states and are not boundary condition specific [Uemura *et al.*, 2012]. Changes in boundary conditions impact the permanence of the evaporative source, precipitation seasonality, and elevation corrections, together with evaporation and condensation processes. Hence, refined equations incorporating further climatic variables (such as relative humidity), or providing boundary condition or seasonally specific coefficients, may reduce the discrepancies between source temperature estimates determined synthetically from MCIM regressions and those simulated here using average values within the VSD. This would be particularly enlightening for Greenland model-proxy comparisons for changes occurring in the LGM experiment.

[57] Second, although GCMs are useful tools for examining isotope-climate relationships because they capture dynamical complexity beyond Rayleigh-type processes, they are, by necessity, only as good as the accuracy of parameterizations (such as kinetic fractionation processes) relative to the real world. The parameterizations of the MCIM and GISS models are different and so conducting MCIM simulations using parameterizations may help resolve the discrepancy in source temperature estimates identified here. Furthermore, model biases, such as poorly resolved inversion layers, excessive accumulation, and warm continental biases, may result in erroneous simulations of polar climates [Schmidt *et al.*, 2007]. Orography in GCMs is strongly dependent on both the model resolution and discretization scheme (Masson-Delmotte *et al.*, 2006). Hence, the model resolution utilized here may be inadequate to resolve critical topography for regional climatologies and a higher-resolution model may improve the simulation of precipitation regimes at sites such as EDC, which is highly sensitive to local and regional-scale topography. An increase in horizontal and vertical model resolution would likely yield improved  $d$  performance over Antarctica [Werner *et al.*, 2011]. In addition, the combined use of  $^{17}\text{O}$ -excess with deuterium excess may help disentangle source effects on isotopic signals [Winkler *et al.*, 2012].

## 7. Conclusions

[58] Using the water isotope-enabled GISS ModelE-R and a novel suite of vapor source distribution tracers, we examine the relationship between deuterium excess variability at high-latitude ice core sites and the climatic conditions prevailing within their moisture source regions. Average modeled source temperature values for various Greenland and Antarctic sites are compared to synthetic values calculated from numerical isotope-temperature relationships (equations (2) and (3); Stenni *et al.* [2001]; Masson-Delmotte *et al.* [2005a]) for a suite of simulations encompassing a range of mean climatic states. These include highly idealized experiments that are included here to assess the rigor of  $d$ -temperature relationships under varying boundary conditions. Similar comparisons are

made with simulated  $d$  changes over ice core site gridboxes and synthetic  $d$  values.

[59] There is a general correspondence between modeled and numerically derived source values for most sites, particularly during the mid-Holocene and ENSO-type climate simulations, indicating that in some simulations and regions,  $d$  is a faithful tracer of temperature variability within a site's evaporative source using MCIM-derived inversions (equations (2) and (3)). Over Greenland sites GRIP and NGRIP, there are larger discrepancies between Tsource estimates occurring during the LGM experiment, particularly in the boreal summer. Simulated LGM climates are characterized by substantial changes in regional circulation under the influence of expanded sea ice and the Laurentide Ice Sheet. The quantification of source temperature fluctuations may be affected by changes in precipitation intermittency and evaporative moisture source origins during the LGM. The disparity of modeled and synthetic estimates of Greenland Tsource changes during the LGM demonstrates the complexity of  $d_p$ -Tsource relationships, particularly under vastly different boundary conditions where specific regression coefficients may be necessary [Uemura *et al.*, 2012]. There are also large discrepancies in comparisons of synthetic and modeled  $d$  changes at the EDC site in Antarctica, which are attributed to regional scale deficiencies in modeled climatologies. Here significant disparities exist between simulated preindustrial climates and local observations, indicating that this high-elevation, topographically complex area requires high spatial resolution modeling to capture realistic climatologies [Masson-Delmotte *et al.*, 2011; Werner *et al.*, 2011]. Conversely, at the lower-elevation EDML site, deuterium excess was found to be a faithful tracer of evaporative source temperatures by the numerical isotope-temperature relationships utilized and is a generally robust proxy throughout a range of different climatic states. At this location, coisotopic approaches are invaluable for reconstructing past changes in the high-latitude hydrological cycle under a broad range of conditions.

[60] There are multiple well-recognized climatic influences on  $d$  variability, including those that drive moisture evaporation, condensation, and transport. We suggest that the closer correspondence of modeled and synthetic source SATs, compared with SST averages, results from the influence of evaporation kinetics on the isotopic composition of water vapor. Changes in relative humidity and wind speed are important climatic influences on isotopic composition, and significant changes in relative humidity are modeled here in different experiments. The exclusion of the influence of humidity changes in MCIM regressions may be a limitation of quantifying source temperature changes from isotopic profiles where large changes in humidity in the source region occur, such as during the LGM. Similarly, continentally derived moisture provides a significant contribution to overall precipitation and its composition, even for high-latitude proxy sites. The apparent importance of a range of climatic controls on evaporation supports results from previous model, experimental, and observational-based studies that highlight the contribution of relative humidity at the ocean surface and the strength of winds to deuterium excess fluctuations.

[61] The climatic changes simulated here in a series of idealized experiments using a relatively coarse horizontal resolution GCM, provide a useful complement to observational and isotopic model-based studies for understanding

deuterium excess as a climate proxy and high-latitude paleo-hydrological processes more generally. Deuterium excess is an integrated tracer of past hydrological changes and records a suite of climatic changes. The numerical equations resulting from simple isotopic models are a simplification of the climate system, and many variables that affect the isotopic composition are not explicitly parameterized. As a proxy,  $d$  is found to be amenable to simplification at some sites and for some types of climatic change. However, variability in other controls of evaporation kinetics, such as humidity and wind speed, or in precipitation seasonality and moisture source region, are also important isotopic influences and these warrant further investigation. Quantitative interpretations of deuterium excess may require caution for some sites at times characterized by significantly different boundary conditions than the present, particularly during the LGM.

[62] **Acknowledgments.** The authors thank NASA GISS for institutional support. NSF ATM 07-53868 supports A.N.L. and travel for S.C.L. This study was assisted by APA/ASS/JAE Scholarships and travel funding from Paterson Fellowship/ANU Vice-Chancellor to S.C.L. The authors also thank two anonymous reviewers, who greatly assisted in improving this manuscript.

## References

- Armengaud, A., R. D. Koster, J. Jouzel, and P. Ciais (1998), Deuterium excess in Greenland snow: Analysis with simple and complex models, *J. Geophys. Res.*, **103**, 8947–8953, doi:10.1029/98jd00274.
- Barlow, L. K., J. C. Rogers, M. C. Serreze, and R. G. Barry (1997), Aspects of climate variability in the North Atlantic sector: Discussion and relation to the Greenland Ice Sheet Project 2 high-resolution isotopic signal, *J. Geophys. Res.*, **102**, 26333–26344, doi:10.1029/96jc02401.
- Berger, A., and M. F. Loutre (1991), Insolation values for the climate of the last 10 million years, *Quaternary Sci. Rev.*, **10**, 297–317, doi:10.1016/0277-3791(91)90033-Q.
- Bromwich, D. H., Z. Guo, L. Bai, and Q.-S. Chen (2004), Modeled Antarctic precipitation. Part I: Spatial and temporal variability, *J. Clim.*, **17**, 427–447, doi:10.1175/1520-0442(2004)017<0427:MAPPIS>2.0.CO;2.
- Brook, E. J., S. Harder, J. Severinghaus, E. J. Steig, and C. M. Sucher (2000), On the origin and timing of rapid changes in atmospheric methane during the Last Glacial Period, *Global Biogeochem. Cycles*, **14**, 559–572, doi:10.1029/1999GB001182.
- Cappa, C. D., M. B. Hendricks, D. J. DePaolo, and R. C. Cohen (2003), Isotopic fractionation of water during evaporation, *J. Geophys. Res.*, **108**, 4525, doi:10.1029/2003jd003597.
- Carlson, A. E., A. N. LeGrande, D. W. Oppo, R. E. Came, G. A. Schmidt, F. S. Anslow, J. M. Licciardi, and E. A. Obbink (2008), Rapid early Holocene deglaciation of the Laurentide Ice Sheet, *Nat. Geosci.*, **1**, 620–624, doi:10.1038/ngeo285.
- Cayan, D. R. (1992), Latent and sensible heat flux anomalies over the northern oceans: The connection to monthly atmospheric circulation, *J. Clim.*, **5**, 354–369, doi:10.1175/1520-0442(1992)005<0354:LASHFA>2.0.CO;2.
- Charles, C. D., D. Rind, J. Jouzel, R. D. Koster, and R. G. Fairbanks (1994), Glacial-interglacial changes in moisture sources for Greenland: Influences on the ice core record of climate, *Science*, **263**, 508–511, doi:10.1126/science.263.5146.508.
- Ciais, P., and J. Jouzel (1994), Deuterium and oxygen 18 in precipitation: Isotopic model, including mixed cloud processes, *J. Geophys. Res.*, **99**, 16,793–16,803, doi:10.1029/94jd00412.
- Clark, P. U., A. S. Dyke, J. D. Shakun, A. E. Carlson, J. Clark, B. Wohlfarth, J. X. Mitrovica, S. W. Hostetler, and A. M. McCabe (2009), The Last Glacial Maximum, *Science*, **325**, 710–714, doi:10.1126/science.1172873.
- Craig, H. (1961), Isotopic variations in meteoric waters, *Science*, **133**, 1702–1703, doi:10.1126/science.133.3465.1702.
- Dahl-Jensen, D., K. Mosegaard, N. Gundestrup, G. D. Clow, S. J. Johnsen, A. W. Hansen, and N. Balling (1998), Past temperatures directly from the Greenland Ice Sheet, *Science*, **282**, 268–271, doi:10.1126/science.282.5387.268.
- Dansgaard, W. (1964), Stable isotopes in precipitation, *Tellus*, **16**, 436–468, doi:10.1111/j.2153-3490.1964.tb00181.x.
- Delaygue, G., V. Masson, J. Jouzel, R. D. Koster, and R. J. Healy (2000), The origin of Antarctic precipitation: A modelling approach, *Tellus B*, **52**, 19–36, doi:10.1034/j.1600-0889.2000.00951.x.
- EPICA Community Members (2006), One-to-one coupling of glacial climate variability in Greenland and Antarctica, *Nature*, **444**, 195–198, doi:10.1038/nature05301.
- Gersonde, R., X. Crosta, A. Abelmann, and L. Armand (2005), Sea-surface temperature and sea ice distribution of the Southern Ocean at the EPILOG Last Glacial Maximum—a circum-Antarctic view based on siliceous microfossil records, *Quaternary Sci. Rev.*, **24**, 869–896, doi:10.1016/j.quascirev.2004.07.015.
- Hansen, J., M. Sato, R. Ruedy, P. Kharecha, A. Lacis, R. Miller, L. Nazarenko, K. Lo, G. A. Schmidt, G. Russell, et al. (2007), Climate simulations for 1880–2003 with GISS modelE, *Clim. Dynam.*, **29**, 661–696, doi:10.1007/s00382-007-0255-8.
- Helsen, M. M., R. S. W. van de Wal, M. R. van den Broeke, V. Masson-Delmotte, H. A. J. Meijer, M. P. Scheele, and M. Werner (2006), Modeling the isotopic composition of Antarctic snow using backward trajectories: Simulation of snow pit records, *J. Geophys. Res.*, **111**, D15109, doi:10.1029/2005jd006524.
- Hoffmann, G., J. Jouzel, and S. Johnsen (2001), Deuterium excess record from central Greenland over the last millennium: Hints of a North Atlantic signal during the Little Ice Age, *J. Geophys. Res.*, **106**, 14,265–14,274, doi:10.1029/2000jd900585.
- Indermuhle, A., T. F. Stocker, F. Joos, H. Fischer, H. J. Smith, M. Wahlen, B. Deck, D. Mastroianni, J. Tschumi, T. Blunier, et al. (1999), Holocene carbon-cycle dynamics based on CO<sub>2</sub> trapped in ice at Taylor Dome, *Antarctica, Nature*, **398**, 121–126, doi:10.1038/18158.
- Johnsen, S., W. Dansgaard, and J. W. C. White (1989), The origin of Arctic precipitation under present and glacial conditions, *Tellus B*, **41**, 452–468, doi:10.1111/j.1600-0889.1989.tb00321.x.
- Jouzel, J., L. Merlivat, and C. Lorius (1982), Deuterium excess in an East Antarctic ice core suggests higher relative humidity at the oceanic surface during the last glacial maximum, *Nature*, **299**, 688–691, doi:10.1038/299688a0.
- Jouzel, J., and L. Merlivat (1984), Deuterium and oxygen 18 in precipitation: Modeling of the isotopic effects during snow formation, *J. Geophys. Res.*, **89**, 11,749–11,757, doi:10.1029/JD089iD07p11749.
- Jouzel, J., R. D. Koster, R. J. Suozzo, G. L. Russell, J. W. C. White, and W. S. Broecker (1991), Simulations of the HDO and H<sub>2</sub><sup>18</sup>O atmospheric cycles using the NASA GISS general circulation model: sensitivity experiments for present-day conditions, *J. Geophys. Res.*, **96**, 7495–7507, doi:10.1029/90jd02663.
- Jouzel, J., F. Vimeux, N. Caillon, G. Delaygue, G. Hoffmann, V. Masson-Delmotte, and F. Parrenin (2003), Magnitude of isotope/temperature scaling for interpretation of central Antarctic ice cores, *J. Geophys. Res.*, **108**, 4361, doi:10.1029/2002jd002677.
- Jouzel, J., M. Stiévenard, S. J. Johnsen, A. Landais, V. Masson-Delmotte, A. Sveinbjornsdottir, F. Vimeux, U. von Grafenstein, and J. W. C. White (2007), The GRIP deuterium-excess record, *Quaternary Sci. Rev.*, **26**, 1–17, doi:10.1016/j.quascirev.2006.07.015.
- Kageyama, M., and P. J. Valdes (2000), Impact of the North American ice-sheet orography on the Last Glacial Maximum eddies and snowfall, *Geophys. Res. Lett.*, **27**, 1515–1518, doi:10.1029/1999gl011274, 2000.
- Kara, A. B., H. E. Hurlburt, and W. Y. Loh (2007), Which near-surface atmospheric variable drives air-sea temperature differences over the global ocean?, *J. Geophys. Res.*, **112**, C05020, doi:10.1029/2006jc003833.
- Kelley, M. (2003), Water tracers and the hydrologic cycle in a GCM, Doctor of Philosophy, Department of Earth and Environmental Sciences, Columbia University, New York.
- Langen, P., and B. Vinther (2009), Response in atmospheric circulation and sources of Greenland precipitation to glacial boundary conditions, *Clim. Dynam.*, **32**, 1035–1054, doi:10.1007/s00382-008-0438-y.
- LeGrande, A. N., and G. A. Schmidt (2009), Sources of Holocene variability of oxygen isotopes in paleoclimate archives, *Clim. Past*, **5**, 441–455, doi:10.5194/cp-5-441-2009.
- Lewis, S. C., A. N. LeGrande, M. Kelley, and G. A. Schmidt (2010), Water vapour source impacts on oxygen isotope variability in tropical precipitation during Heinrich events, *Clim. Past*, **6**, 325–343, doi:10.5194/cp-6-325-2010.
- Licciardi, J. M., P. U. Clark, J. W. Jenson, and D. R. Macayeal (1998), Deglaciation of a soft-bedded Laurentide Ice Sheet, *Quaternary Sci. Rev.*, **17**, 427–448, doi:10.1016/S0277-3791(97)00044-9.
- Luz, B., E. Barkan, R. Yam, and A. Shemesh (2009), Fractionation of oxygen and hydrogen isotopes in evaporating water, *Geochim. Cosmochim. Acta*, **73**, 6697–6703, doi:10.1016/j.gca.2009.08.008.
- MARGO Project Members (2009), Constraints on the magnitude and patterns of ocean cooling at the Last Glacial Maximum, *Nat. Geosci.*, **2**, 127–132, doi:10.1038/ngeo411.
- Masson-Delmotte, V., B. Stenni, and J. Jouzel (2004), Common millennial-scale variability of Antarctic and Southern Ocean temperatures during the past 5000 years reconstructed from the EPICA Dome C ice core, *The Holocene*, **14**, 145, doi:10.1191/0959683604hl697ft.

- Masson-Delmotte, V., J. Jouzel, A. Landais, M. Stievenard, S. J. Johnsen, J. W. C. White, M. Werner, A. Sveinbjornsdottir, and K. Fuhrer (2005a), GRIP deuterium excess reveals rapid and orbital-scale changes in Greenland moisture origin, *Science*, *309*, 118–121, doi:10.1126/science.1108575.
- Masson-Delmotte, V., A. Landais, M. Stievenard, O. Cattani, S. Falourd, J. Jouzel, S. J. Johnsen, D. Dahl-Jensen, A. Sveinbjornsdottir, J. W. C. White, et al. (2005b), Holocene climatic changes in Greenland: Different deuterium excess signals at Greenland Ice Core Project (GRIP) and NorthGRIP, *J. Geophys. Res.*, *110*, doi:10.1029/2004jd005575.
- Masson-Delmotte, V., M. Kageyama, P. Braconnot, S. Charbit, G. Krinner, C. Ritz, E. Guilyardi, J. Jouzel, A. Abe-Ouchi, M. Crucifix, et al. (2006), Past and future polar amplification of climate change: climate model intercomparisons and ice-core constraints, *Clim. Dyn.*, *26*, 513–529, doi:10.1007/s00382-005-0081-9.
- Masson-Delmotte, V., S. Hou, A. Ekaykin, J. Jouzel, A. Aristarain, R. T. Bernardo, D. Bromwich, O. Cattani, M. Delmotte, S. Falourd, et al. (2008), A review of Antarctic surface snow isotopic composition: Observations, atmospheric circulation, and isotopic modeling, *J. Clim.*, *21*, 3359–3387, doi:10.1175/2007JCLI2139.1.
- Masson-Delmotte, V., D. Buiron, A. Ekaykin, M. Frezzotti, H. Gallée, J. Jouzel, G. Krinner, A. Landais, H. Motoyama, H. Oerter, et al. (2011), A comparison of the present and last interglacial periods in six Antarctic ice cores, *Clim. Past*, *7*, 397–423, doi:10.5194/cp-7-397-2011.
- Merlivat, L., and J. Jouzel (1979), Global climatic interpretation of the deuterium-oxygen 18 relationship for precipitation, *J. Geophys. Res.*, *84*, 5029–5033, doi:10.1029/JC084iC08p05029.
- Noone, D. (2008), The influence of midlatitude and tropical overturning circulation on the isotopic composition of atmospheric water vapor and Antarctic precipitation, *J. Geophys. Res.*, *113*, D04102, doi:10.1029/2007JD008892.
- North Greenland Ice Core Project members (2004), High-resolution record of Northern Hemisphere climate extending into the last interglacial period, *Nature*, *431*, 147–151, doi:10.1038/nature02805.
- Otto-Bliessner, B. L., C. D. Hewitt, T. M. Marchitto, E. Brady, A. Abe-Ouchi, M. Crucifix, S. Murakami, and S. L. Weber (2007), Last Glacial Maximum ocean thermohaline circulation: PMIP2 model intercomparisons and data constraints, *Geophys. Res. Lett.*, *34*, L12706, doi:10.1029/2007gl029475.
- Peltier, W. R. (2004), Global glacial isostasy and the surface of the ice-age earth: The ICE-5G (VM2) model and GRACE, *Annu. Rev. Earth Planet. Sci.*, *32*, 111–149, doi:10.1146/annurev.earth.32.082503.144359.
- Reynolds, R. W., and T. M. Smith (1994), Improved global sea surface temperature analyses using optimum interpolation, *J. Clim.*, *7*, 929–948, doi:10.1175/1520-0442(1994)007<0929:IGSSTA>2.0.CO;2.
- Ruiz-Barradas, A., and S. Nigam (2006), Great Plains hydroclimate variability: The view from North American regional reanalysis, *J. Clim.*, *19*, 3004–3010, doi:10.1175/JCLI3768.1.
- Schlosser, E., H. Oerter, V. Masson-Delmotte, C. Reijmer (2008), Atmospheric influence on the deuterium excess signal in polar firn: implications for ice-core interpretation, *J. Glaciol.*, *54*, 117–124, doi:10.3189/002214308784408991.
- Schmidt, G. A., G. Hoffmann, D. T. Shindell, and Y. Y. Hu (2005), Modeling atmospheric stable water isotopes and the potential for constraining cloud processes and stratosphere-troposphere water exchange, *J. Geophys. Res.*, *110*, D21314, doi:10.1029/2005JD005790.
- Schmidt, G. A., R. Ruedy, J. E. Hansen, I. Aleinov, N. Bell, M. Bauer, S. Bauer, B. Cairns, V. Canuto, Y. Cheng, et al. (2006), Present-day atmospheric simulations using GISS ModelE: Comparison to in situ, satellite, and reanalysis data, *J. Clim.*, *19*, 153–192, doi:10.1175/JCLI3612.1171.
- Schmidt, G. A., A. N. LeGrande, and G. Hoffmann (2007), Water isotope expressions of intrinsic and forced variability in a coupled ocean-atmosphere model, *J. Geophys. Res.*, *112*, D10103, doi:10.1029/2006JD007781.
- Sodemann, H., C. Schwierz, and H. Wernli (2008), Interannual variability of Greenland winter precipitation sources: Lagrangian moisture diagnostic and North Atlantic Oscillation influence, *J. Geophys. Res.*, *113*, D03107, doi:10.1029/2007jd008503.
- Sodemann, H., and A. Stohl (2009), Asymmetries in the moisture origin of Antarctic precipitation, *Geophys. Res. Lett.*, *36*, L22803, doi:10.1029/2009gl040242.
- Song, X., and L. Yu (2012), High-latitude contribution to global variability of air-sea sensible heat flux, *J. Clim.*, *25*, 3515–3531, doi:10.1175/jcli-d-11-00028.1.
- Sowers, T., R. B. Alley, and J. Jubenville (2003), Ice core records of atmospheric N<sub>2</sub>O covering the last 106,000 years, *Science*, *301*, 945–948, doi:10.1126/science.108529.
- Steffensen, J. P., K. K. Andersen, M. Bigler, H. B. Clausen, D. Dahl-Jensen, H. Fischer, K. Goto-Azuma, M. Hansson, S. J. Johnsen, J. Jouzel, et al. (2008), High-resolution Greenland ice core data show abrupt climate change happens in few years, *Science*, *321*, 680–684, doi:10.1126/science.1157707.
- Stenni, B., V. Masson-Delmotte, S. Johnsen, J. Jouzel, A. Longinelli, E. Monnin, R. Röthlisberger, and E. Selmo (2001), An oceanic cold reversal during the last deglaciation, *Science*, *293*, 2074–2077, doi:10.1126/science.1059702.
- Stenni, B., J. Jouzel, V. Masson-Delmotte, R. Röthlisberger, E. Castellano, O. Cattani, S. Falourd, S. J. Johnsen, A. Longinelli, J. P. Sachs, et al. (2004), A late-glacial high-resolution site and source temperature record derived from the EPICA Dome C isotope records (East Antarctica), *Earth Planet. Sci. Lett.*, *217*, 183–195, doi:10.1016/S0012-821X(03)00574-0.
- Stenni, B., V. Masson-Delmotte, E. Selmo, H. Oerter, H. Meyer, R. Röthlisberger, J. Jouzel, O. Cattani, S. Falourd, H. Fischer, et al. (2010), The deuterium excess records of EPICA Dome C and Dronning Maud Land ice cores (East Antarctica), *Quaternary Sci. Rev.*, *29*, 146–159, doi:10.1016/j.quascirev.2009.10.009.
- Stouffer, R. J., J. Yin, J. M. Gregory, K. W. Dixon, M. J. Spelman, W. Hurlin, A. J. Weaver, M. Eby, G. M. Flato, H. Hasumi, et al. (2006), Investigating the causes of the response of the thermohaline circulation to past and future climate changes, *J. Clim.*, *19*, 1365–1387, doi:10.1175/JCLI3689.1.
- Uemura, R., Y. Matsui, K. Yoshimura, H. Motoyama, and N. Yoshida (2008), Evidence of deuterium excess in water vapor as an indicator of ocean surface conditions, *J. Geophys. Res.*, *113*, D19114, doi:10.1029/2008jd010209.
- Uemura, R., V. Masson-Delmotte, J. Jouzel, A. Landais, H. Motoyama, and B. Stenni (2012), Ranges of moisture-source temperature estimated from Antarctic ice cores stable isotope records over glacial-interglacial cycles, *Clim. Past*, *8*, 1109–1125, doi:10.5194/cp-8-1109-2012.
- Vimeux, F., V. Masson, G. Delaygue, J. Jouzel, J. R. Petit, and M. Stievenard (2001), A 420,000 year deuterium excess record from East Antarctica: Information on past changes in the origin of precipitation at Vostok, *J. Geophys. Res.*, *106*, 31,863–31,873, doi:10.1029/2001jd900076.
- Vimeux, F., K. M. Cuffey, and J. Jouzel (2002), New insights into Southern Hemisphere temperature changes from Vostok ice cores using deuterium excess correction, *Earth Planet. Sci. Lett.*, *203*, 829–843, doi:10.1016/S0012-821X(02)00950-0.
- Werner, M., U. Mikolajewicz, M. Heimann, and G. Hoffmann (2000), Borehole versus isotope temperatures on Greenland: Seasonality does matter, *Geophys. Res. Lett.*, *27*, 723–726, doi:10.1029/1999gl006075.
- Werner, M., M. Heimann, and G. Hoffmann (2001), Isotopic composition and origin of polar precipitation in present and glacial climate simulations, *Tellus B*, *53*, 53–71, doi:10.1034/j.1600-0889.2001.01154.x.
- Werner, M., P. M. Langebroek, T. Carlsen, M. Herold, and G. Lohmann (2011), Stable water isotopes in the ECHAM5 general circulation model: Toward high-resolution isotope modeling on a global scale, *J. Geophys. Res.*, *116*, D15109, doi:10.1029/2011jd015681.
- Winkler, R., A. Landais, H. Sodemann, L. Dümbgen, F. Prié, V. Masson-Delmotte, B. Stenni, and J. Jouzel (2012), Deglaciation records of 17O-excess in East Antarctica: Reliable reconstruction of oceanic normalized relative humidity from coastal sites, *Clim. Past*, *8*, 1–16, doi:10.5194/cp-8-1-2012.
- Xie, P., and P. A. Arkin (1996), Analyses of global monthly precipitation using gauge observations, satellite estimates, and numerical model predictions, *J. Clim.*, *9*, 840–858, doi:10.1175/1520-0442(1996)009.